An assessment of the tropospherically accessible photo-initiated ground state chemistry of carbonyls

Keiran N. Rowell[1,2], Scott H. Kable[2], and Meredith J. T. Jordan[1]

[1]School of Chemistry, University of Sydney, Sydney, Australia
[2]School of Chemistry, University of New South Wales, Sydney, Australia

Correspondence: Meredith Jordan (meredith.jordan@sydney.edu.au)

Abstract. Carbonyls are among the most abundant volatile organic compounds in the atmosphere. They are central to atmospheric photochemistry as absorption of near-UV radiation by the C=O chromophore can lead to photolysis. If photolysis does not occur on electronic excited states, non-radiative relaxation to the ground state will form carbonyls with extremely high internal energy. These 'hot' molecules can access a range of ground state reactions. Up to nine potential ground state reactions are investigated at the B2GP-PLYP-D3/def2-TZVP level of theory for a dataset of 20 representative carbonyls. Almost all are energetically accessible under tropospheric conditions. Comparison with experiment suggests the most significant ground state dissociation pathways will be concerted triple fragmentation in saturated aldehydes, Norrish type III dissociation to form another carbonyl, and H_2–loss involving the formyl H atom in aldehydes. Tautomerisation, leading to more reactive unsaturated species, is also predicted to be energetically accessible and is likely to be important when there is no low-energy ground state dissociation pathway, for example in α,β-unsaturated carbonyls and some ketones. The concerted triple fragmentation and H_2–loss pathways have immediate atmospheric implication to global H_2 production and tautomerisaton has implication to the atmospheric production of organic acids.

1   Introduction

Carbonyls are a class of volatile organic compounds (VOCs) central to atmospheric chemistry. They arise, in large quantities, from primary anthropogenic and biogenic emissions and via secondary atmospheric processes (Kesselmeier and Staudt, 1999; Millet et al., 2010; Chen et al., 2014). For example, small carbonyls, such as acetone, formaldehyde and acetaldehyde, which are ranked in the top 25 of all anthropogenically emitted molecules by mass (Simon et al., 2010), are emitted as pollutants (Chen et al., 2014). Up to 10% of carbon initially fixed by plants is also subsequently emitted as biological volatile organic compounds (BVOCs), which include directly emitted carbonyls as well as other volatile species that are subsequently oxidised to carbonyls (Seco et al., 2007). Indeed, carbonyls are generated throughout the oxidative degradation pathways of all VOCs (Carlier et al., 1986; Atkinson and Arey, 2003). Atmospheric concentrations of carbonyls are in the pptV-ppbV range (Tanner et al., 1996), with high concentrations found at low altitudes and in polluted environments (Lee et al., 1998; Pal et al., 2008; Guo et al., 2014; Menchaca-Torre et al., 2015).
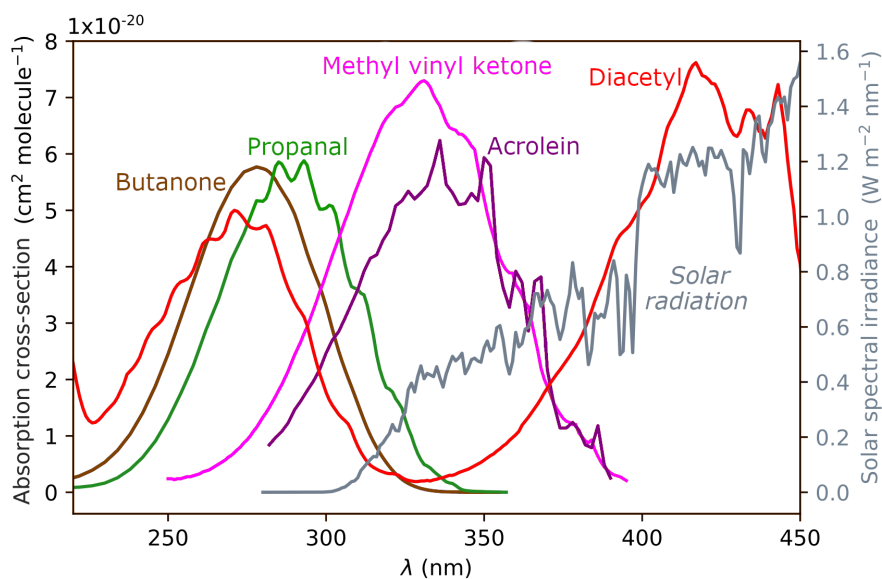
Figure 1. UV absorption spectra of representative carbonyls: aldehydes (represented by propanal), ketones (butanone), enals (acrolein), enones (methyl vinyl ketone), and α-dicarbonyls (diacetyl). The solar spectrum is shown in grey, plotted against the right ordinate.

There are of the order of 10^6 known or suspected VOCs in the atmosphere (Goldstein and Galbally, 2007). As a category,
25 BVOCs are structurally complex and carbonyls formed by their subsequent oxidation will reflect this structural diversity. Consequently, atmospheric carbonyls can have varied chemical structures and reactivities (Kawamura et al., 2000; Atkinson et al., 2006). Structural complexities include double-bonds, branched carbon chains and varied functionalisation. The atmospheric importance of carbonyls arises because they are one of the few classes of VOC that can efficiently absorb solar radiation in the troposphere. In the atmosphere, carbonyl photochemistry is most notable for its generation of radicals following excited state
30 bond cleavage, the Norrish Type I reaction (NTI) (Norrish and Appleyard, 1934), and these radicals drive key atmospheric reactions (Lary and Shallcross, 2000; Yang et al., 2018). However, many other reactions, including reactions on the ground electronic state, S_0, are possible.

The intensity of solar radiation reaching the troposphere is shown in gray on the right axis of Fig. 1. Most UV-B radiation (280–315 nm) is absorbed by the ozone layer, and the intensity of UV-A radiation (315-400 nm) increases with increasing
35 wavelength. The maximum photon energy available in the troposphere is $\sim$400 kJ/mol (300 nm) and is shown in violet on relevant energetic plots below. The overlap of a given carbonyl absorption spectrum and the solar spectrum defines the actinic energy window in which photo-initiated chemistry can occur. In carbonyls, a near-UV photon excites the $S_1 \leftarrow S_0\,(n, \pi^*)$ transition of the C=O chromophore. The absorption wavelength depends on the structural class of the carbonyl and is determined by the substituents attached to the C=O. UV absorption spectra for representative carbonyls are shown in Fig. 1.

40   Over the past couple of decades, it has become apparent that there are carbonyl "photochemical" pathways on the ground electronic state (S_0). These photo-initiated reactions on S_0 include the novel class of 'roaming' reactions (Townsend et al., 2004; Bowman and Houston, 2017), where partly dissociated radical fragments become trapped in each other's van der Waals well and recombine to generate molecular products. However, more conventional S_0 transition state (TS) reactions, which occur over a barrier, as well as barrierless S_0 reactions, are also being discovered (Heazlewood et al., 2011; So et al., 2018; Toulson

45 et al., 2018). Despite the growing evidence of carbonyl ground state reactions, following excitation at energies accessible in the troposphere ($\lambda > 300$ nm), these reactions are almost entirely absent from the reaction schemes of contemporary atmospheric models (Wild et al., 2000; Rickard and Young; Jenkin et al., 1997, 2002; Bey et al., 2001).

1.1   The Tropospheric Fate of Carbonyls

The tropospheric fate of an illustrative carbonyl, acetaldehyde (CH_3CHO) is shown schematically in Fig. 2. A near-UV photon

50 excites the $S_1 \leftarrow S_0$ (n, π^*) transition. The actinic absorption window, indicated in Fig. 2 by violet shading, is bounded by the lowest energy excitation to S_1 and the highest energy photon available in the troposphere. For most carbonyls the S_1 state is bound at actinic energies, as shown in Fig. 2, and S_1 reactions are inaccessible (Haas, 2004; Rowell et al., 2019). Intersystem crossing (ISC) from S_1 to the lowest energy triplet state, T_1, is formally spin-forbidden, however, as shown schematically in Fig. 2, carbonyl S_1 and T_1 minimum energy geometries are almost identical and the energetic separation between them is

55 small. This allows relatively fast $S_1 \rightarrow T_1$ ISC (Hansen and Lee, 1975), indicated in Fig. 2 by a thick ISC arrow. On T_1, NTI α-bond cleavage is the most common photolysis reaction (Kirkbride and Norrish, 1931; Zhu et al., 2009) and we define NTIa and NTIb as cleavage of the α-bond to the larger and smaller substituents, respectively. In CH_3CHO NTIa results in formation of $^\bullet CH_3 + {}^\bullet HCO$ and NTIb yields $CH_3CO^\bullet + {}^\bullet H$. On T_1 both NTIa and NTIb involve an energetic barrier, shown in orange in Fig. 2.

60   For larger carbonyls, the Norrish Type II (NTII) intramolecular hydrogen-transfer reaction, forming an alkene and an enol, also occurs and is initiated in an electronic excited state (Tadić et al., 2002, 2012). Although NTI and NTII are typically the major contributors to the photolysis quantum yield (QY) of carbonyls (Wagner and Zepp, 1972; Wagner and Klán, 2004; Zhu et al., 2009), if excitation is to energies below excited state photolysis thresholds, or if the electronically excited carbonyl is collisionally cooled below these thresholds, non-radiative relaxation to S_0 must occur; fluorescence and phosphorescence QYs

65 in carbonyls are typically <1% (Heicklen and Noyes, 1959; Copeland and Crosley, 1985). The large energy separation between S_1 and S_0 means $S_1 \rightarrow S_0$ internal conversion (IC) will be slow and less important than ISC (Lee and Chen, 1997). Indeed, rapid IC is usually associated with conical intersections: geometric configurations where two electronic surfaces are degenerate (Schuurman and Stolow, 2018). In the main, these lie above the actinic energy range in carbonyls (Diau et al., 2001; Chen and Fang, 2009; Toulson et al., 2017).

70   The carbonyl RC=O group is planar in the S_0 minimum energy geometry but pyramidalised in the S_1 and T_1 minima (Godunov et al., 1995). The change in electron spin, geometric dissimilarity and energetic separation between the T_1 and S_0 minima suggest $T_1 \rightarrow S_0$ ISC may be slow. However, the non-bonding oxygen lone pair orbital, n, in C=O is approximately orthogonal to the antibonding π^* excited state orbital. Thus the change in electron spin angular momentum in $T_1 \rightarrow S_0$ relax-
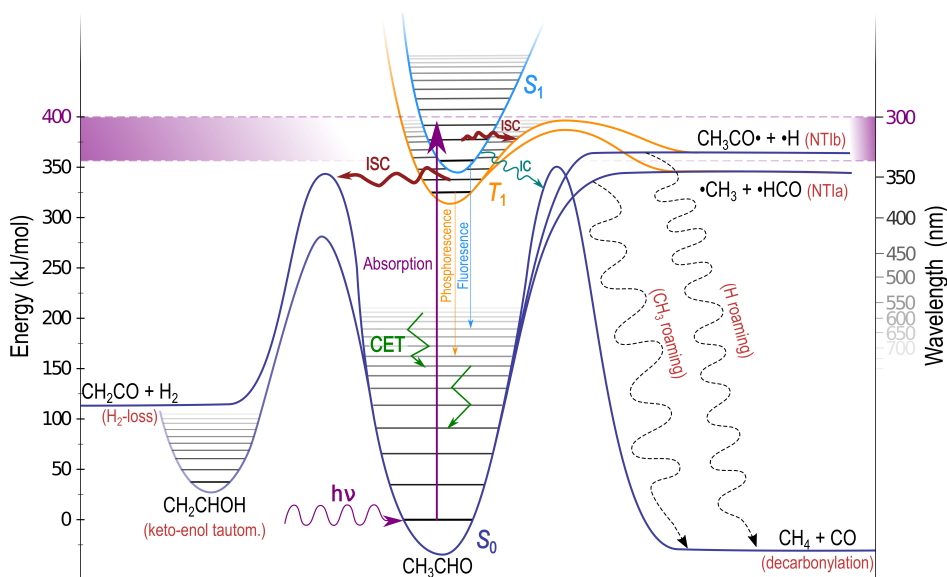
Figure 2. Schematic of the atmospheric fate of acetaldehyde (CH₃CHO) following absorption of a near-UV photon. Possible outcomes depend on excitation energy and include: electronic surface crossing, collisional energy transfer (CET), unimolecular dissociation including roaming (dashed arrows), and isomerisation.

ation is accompanied by a change in electron orbital angular momentum. This results in conservation of total electron angular momentum and a high $T_1 \rightarrow S_0$ ISC rate, as dictated by El-Sayed's rule (El-Sayed, 1961). Indeed, ISC to S_0 can be kinetically competitive even when NTI reactions are accessible (Heazlewood et al., 2009; Amaral et al., 2010).

The most likely carbonyl relaxation route to S_0 is therefore via two sequential ISC steps (Toulson et al., 2017). This generates vibrationally 'hot' photo-excited S_0 molecules that retain much of the initial UV photon energy as internal energy. This 'hot' carbonyl can collide with other atmospheric molecules and collisional energy transfer (CET) removes excess vibrational energy, returning the molecule to thermal equilibrium. This is indicated in Fig. 2 by angular green arrows in the S_0 well, although CET will also occur in S_1, T_1 and isomer wells (Heazlewood et al., 2011; Andrews et al., 2012). The photo-excited S_0 carbonyls are conformationally flexible, and S_0 dissociation and isomerisation will compete with CET.

This paper explores, using computational chemistry, the possible S_0 dissociation and isomerisation pathways and how they depend on the structural class of the carbonyl.

1.2 The Dataset

There are a vast number of carbonyls in the atmosphere with little experimental data in comparison to this diversity (Atkinson et al., 1992). Here we consider a dataset of 20 carbonyls, which includes the 12 species that have explicit photolysis reactions within the Master Chemical Mechanism (Jenkin et al., 1997; Rickard and Young) and five species in the GEOS-Chem (Bey et al., 2001) atmospheric chemistry models. We also include carbonyls with atmospherically representative structural features

90 based on bond order or substitution around the C=O chromophore. The 20 carbonyls in the dataset are shown in Fig. 3 and were previously used in a study of excited state NTI photolysis (Rowell et al., 2019). They are colour-coded into seven structurally distinct classes, which determine their absorption spectra (Fig. 1) and chemical behaviour (Atkinson et al., 1992).
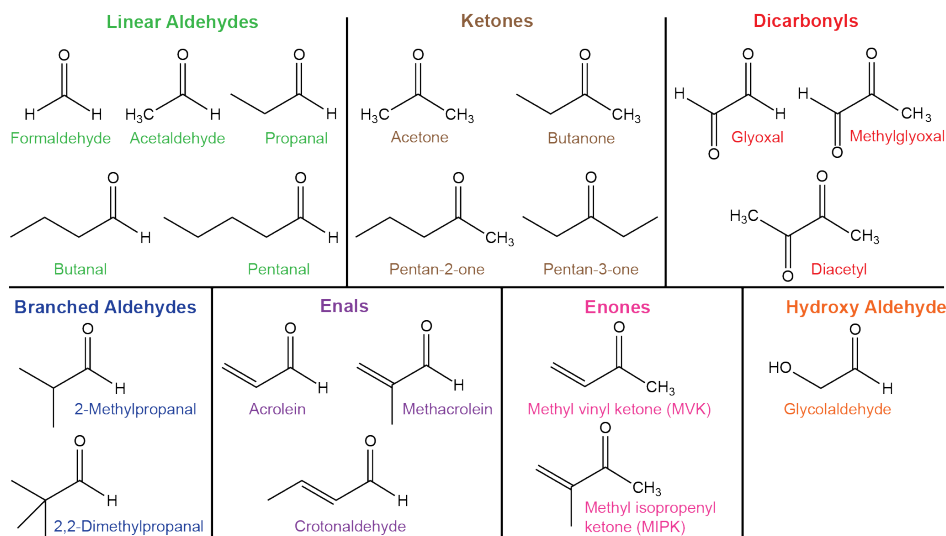

Figure 3. The 20 carbonyls in the dataset, colour-coded according to carbonyl class.

Quantum chemistry methods are used to calculate reaction thresholds for up to nine S_0 unimolecular reactions that may be accessible under tropospheric conditions. . In our quantum chemistry calculations, the threshold is defined as the limiting zero-point corrected electronic energy for the reaction to occur. Experimental thresholds are the lowest energies for which reaction has been observed to occur and hence include tunnelling through any barrier to reaction. In the figures below, the nine possible unimolecular reactions are colour-coded according to Scheme 3. Explicitly, the reactions are:

- Decarbonylation (CO–loss).

- Concerted triple fragmentation (TF).

- Norrish Type III β-H transfer (NTIII).

- H_2–loss from hydrogens at the formyl and α positions (formyl+α).

- H_2–loss from hydrogens at the α and β positions (α+β).

- H_2–loss from hydrogens at the β and γ positions (β+γ).

- Alkane/alkene elimination (AE) in saturated/unsaturated ketones.

- Keto–enol tautomerisation.

- Enal–ketene tautomerisation.

Ground state NTI reactions are also possible for all carbonyls in the dataset. These reactions are barrierless and their asymptotic energies have been previously reported (Rowell et al., 2019). Other isomerisations are possible. For example, acetaldehyde can isomerise to oxirane or methylhydroxycarbene. Although these isomers are theoretically accessible at actinic energies, their formation barriers are very high with low barriers for the reverse isomerisation (Heazlewood et al., 2011). Thus they are unlikely to be collisionally stabilised before isomerising back to the parent carbonyl. Norrish type II reactions are possible for butanal, pentanal and pentan-2-one and have not been considered here as they involve excited electronic states (Tadić et al., 2002, 2012).

Seven of the S_0 reactions listed above are illustrated for butanal in Fig. S1 of the Supplementary Material; alkane elimination is only available to ketones and enal–ketene tautomerisation is only available to acrolein, methacrolein and crotonaldehyde. The figure also includes schematic representations of the concerted TF and NTIII mechanisms.

The calculated S_0 thresholds are used to determine general energetic trends that can be applied to larger carbonyls and to identify the most likely S_0 reactions for each class of carbonyl under tropospheric conditions. These reactions are then assessed in terms of their tropospheric significance. Ultimately, however, the most important reactions will be those with the highest reaction rate coefficients. Although the threshold energy is, in general, the largest contributor to the magnitude of a reaction rate coefficient, entropy is also important. For similar thresholds, reactions with loose transition states, for example, the variational transition states associated with barrierless reactions like the S_0 NTI reactions, will have higher rate coefficients. By identifying reactions that may be important we will be able to focus future work on calculating their reaction rate coefficients and incorporating them into tropospheric master equation models.

2 Computational Methods

S_0 calculations were performed with the B2GP-PLYP double-hybrid density functional (Karton et al., 2008), using the def2-TZVP canonical basis set (Weigend and Ahlrichs, 2005) and the RIJK resolution of the identity approximation with the def2/JK and def2-TZVP/C auxiliary basis sets. The use of the RIJK approximation, and the 'RI-' prefix, are taken as implicit. All calculations were dispersion-corrected using the D3(BJ) scheme (Grimme et al., 2010, 2011), abbreviated D3 below. Geometry optimisations and frequency calculations were performed using the ORCA electronic structure program (Neese, 2017). All zero-point energies were scaled with the literature scaling factor of 0.9752 (Kesharwani et al., 2015).

The B2GP-PLYP functional has been found to give errors <8 kJ/mol across a diverse range of benchmark data (Karton et al., 2008). B2GP-PLYP-D3/def2-TZVP was also validated by the authors against experimental carbonyl T_1 photolysis data, with mean absolute deviations of ∼6 kJ/mol (Rowell et al., 2019). Comparisons of our B2GP-PLYP-D3/def2-TZVP thresholds with previous literature are provided in Tables S1–S6 of Supplementary Material and indicate excellent agreement with high-level correlated methods using accurate geometries. Note that, for S_0 energy differences between structurally similar molecules, as studied here, relative errors would be expected to be lower, approaching 4 kJ/mol 'chemical accuracy' (Pople, 1999).

Transition states were confirmed as first-order saddle points with a single imaginary frequency. Intrinsic reaction coordinate (IRC) calculations were performed to ensure that the normal mode corresponding to the imaginary frequency connected the desired reactant and product minima. In order to reduce computational burden, IRC calculations were not performed where a TS had a structure and reaction coordinate directly analogous to a homologous molecule for which the reaction mechanism had been verified.

Schematic representation of the optimised saddle point structures are shown in the figures below. They are also represented in Figs S2 – S7 and their Cartesian coordinates are provided as Supplementary Material. In general, only the lowest energy thresholds for each reaction class are discussed below, higher energy thresholds are reported as Supplementary Material.

3 Results and Discussion

The lowest energy calculated reaction thresholds for the up to nine S_0 reactions considered are reported in Table 1 for carbonyls in the dataset. Additional, higher energy, thresholds are reported as Supplementary Material. For some of the carbonyls considered, asymptotic energies for NTI reactions can be obtained from (effectively) experimental enthalpies of formation at 0 K, tabulated in the Active Thermochemical Tables (Ruscic et al., 2005; Ruscic, B. and Bross, D. H., 2020). The results in Table 1 with uncertainties are based on these experimental enthalpies of formation. The remaining NTI asymptotic energies shown in Table 1 have been previously calculated and are reproduced from Rowell et al. (2019).

Each reaction type is discussed separately below, with the three H_2–loss reactions discussed together. These data and available literature and experimental results are then analysed to determine chemically rationalised trends that will be applicable to larger carbonyls.

3.1 Decarbonylation (CO–loss)

Decarbonylation, the unimolecular loss of a CO molecule, is uncommon in gas-phase ketones. It has been observed in acetone, although the mechanism is unclear; Skorobogatov et al. (2002) postulated a direct mechanism, presumably via a TS, and roaming reactions have also been suggested in acetone (Goncharov et al., 2008; Saheb and Zokaie, 2018). Here, like previous studies (Saheb and Zokaie, 2018; So et al., 2018), we find no computational evidence for direct decarbonylation TSs in ketones.

In aldehydes, the formyl hydrogen is transferred to the main alkyl chain, forming CO and an alkane: R–(C=O)–H → CO + RH. Both roaming and TS decarbonylation mechanisms have been observed in gas-phase reactions of small aldehydes (Townsend et al., 2004; Houston and Kable, 2006; Heazlewood et al., 2008; Rubio-Lago et al., 2012; Yang et al., 2020). Figure 4 shows TS decarbonylation thresholds for the aldehydes in the dataset.

One trend apparent in Fig. 4 is that extension of the alkyl chain has little effect on decarbonylation threshold, with formaldehyde through pentanal all predicted to have ~350 kJ/mol thresholds. The predicted decrease in threshold upon branching at the α-position is <5 kJ/mol.

Table 1. Lowest energy zero-point vibrational energy corrected B2GP-PLYP-D3/def2-TZVP S_0 thresholds (kJ/mol) for the indicated unimolecular reactions of the carbonyls in the dataset (see text).

	CO–loss	TF	NTIII	H$_2$–loss (H positions) (formyl+α)	(α+β)	(β+γ)	AE	Tautomerisation Keto–enol	Enal–ketene	Asymptotic[a] NTIa	NTIb
Aldehydes:											
Formaldehyde	352	–	–	–	–	–	–	–	–	362.8±0.1[b]	362.8±0.1[b]
Acetaldehyde	352	–	–	337	–	–	–	281	–	346.4±0.3[b]	367.8±0.4[b]
Propanal	348	295	332	314	426	–	–	278	–	343.8±0.4[b]	356[c]
Butanal	351	299	311	320	410	516	–	282	–	341[c]	360[c]
Pentanal	350	294	310	317	409	499	–	281	–	345[c]	362[c]
2-Methylpropanal	345	304	330	310	422	–	–	296	–	332[c]	358[c]
2,2-Dimethylpropanal	342	306	322	–	–	–	–	–	–	329[c]	358[c]
Ketones:											
Acetone	–	–	–	–	–	–	363	275	–	346.6±0.5[b]	346.6±0.5[b]
Butanone	–	–	354	–	447	–	351	274	–	344.7±1.0[b]	346[c]
Pentan-2-one	–	–	316	–	416	513	347	270	–	338[c]	342[c]
Pentan-3-one	–	–	350	–	442	–	347	276	–	342[c]	342[c]
α,β-Unsaturated:											
Acrolein	360	343	394	373	–	–	–	291	293	397.9±1.2[b]	352[c]
Crotonaldehyde	375	351	387	386	–	–	–	133[d]	292	412[c]	363[c]
Methacrolein	362	338	379	–	–	–	–	–	285	381[c]	363[c]
Methyl vinyl ketone	–	–	417	–	–	–	329	270	–	393.4±1.0[b]	338[c]
MIPK	–	–	395	–	–	–	334	–	–	376[c]	343[c]
Dicarbonyls:											
Glyoxal	225[e]	247[f]	–	–	–	–	–	–	–	290.5±0.6[b]	360.2±1.4[b]
Methylglyoxal	235[g]	330	400	–	–	–	–	–	–	293[c]	354[c]
Diacetyl	–	–	415	–	–	–	–	–	–	303.9±0.8[b]	346[c]
Hydroxy-aldehyde:											
Glycolaldehyde	345	229[h]	–	292	384[i]	–	–	272	–	310[c]	358[c]

a: NTIa and NTIb are cleavage to the larger and smaller fragments, respectively. *b*: Values with uncertainties are determined from experimental enthalpies of formation from the Active Thermochemical Tables (v. 1.22p) (Ruscic, B. and Bross, D. H., 2020; Ruscic et al., 2005); *c*: reproduced from Rowell et al. (2019); *d*: for a [1,5]-H atom shift to form but-1,3-dien-1-ol; *e*: for formation of formaldehyde + CO; *d*: for a 4-centre TS involving the two formyl H atoms; *f*: for formation of acetaldehyde + CO; *g*: The β-H for the TF transition state is from the OH moiety; *h*: The β-H for the TF transition state is from the OH moiety; *i*: The H$_2$–loss TS involves the OH hydrogen.

The decarbonylation thresholds in the α,β-unsaturated enals, acrolein and methacrolein, are ∼10 kJ/mol higher than those for saturated aldehydes, as decarbonylation involves breaking a resonance stabilised C–C bond. Further delocalisation of the π system increases the threshold to 375 kJ/mol for crotonaldehyde.
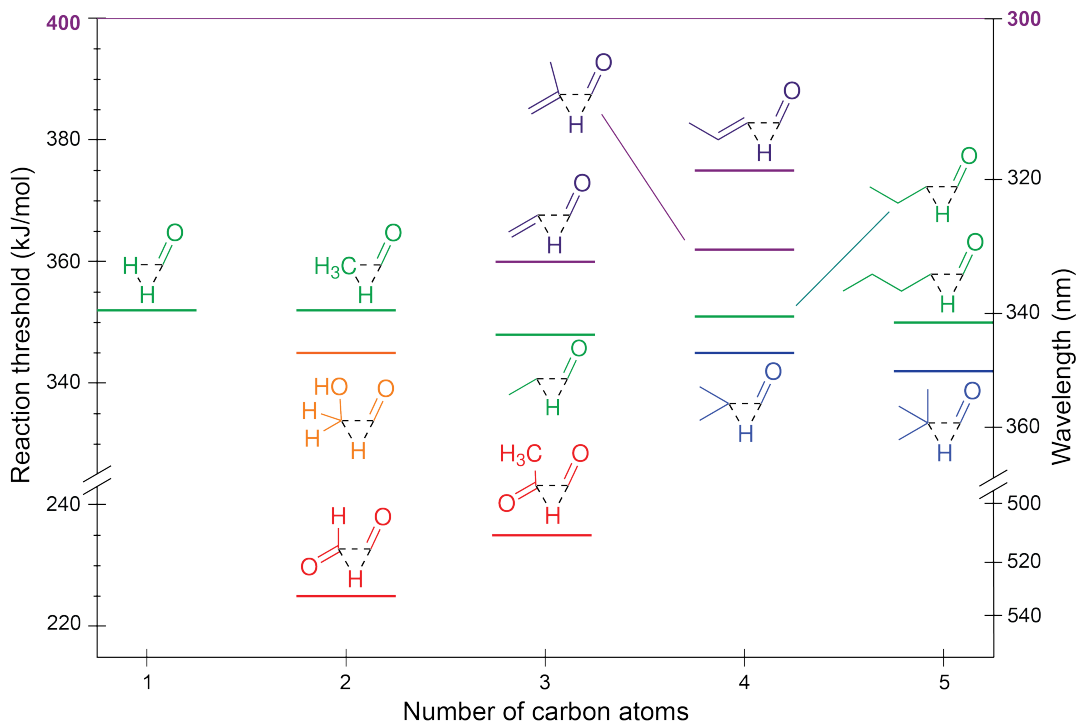
Figure 4. Zero-point vibrational energy corrected B2GP-PLYP-D3/def2-TZVP S_0 decarbonylation thresholds.

The α-dicarbonyls are predicted to have the lowest decarbonylation thresholds, which is consistent with the two electron-withdrawing oxygen substituents reducing the electron density between the carbonyl moieties and weakening the α-C–C bond. Four decarbonylation thresholds were found for glyoxal (Table S1 and Fig. S3 in Sect. S2 of the Supplementary Material) with the lowest energy threshold of 225 kJ/mol corresponding to a non-planar TS and formation of formaldehyde and CO. 175 This threshold is lower than the 251 kJ/mol threshold to form hydroxymethylene, HOCH, and CO. A similar non-planar TS is found for decarbonylation in methylglyoxal to form acetaldehyde, which has a slightly higher threshold of 235 kJ/mol. Here, substitution strengthens the central C–C bond due to electron-donation from the CH$_3$ substituent and there is also a steric penalty at the TS (Fig. S3a *vs.* S3e).

All calculated decarbonylation thresholds are accessible at the maximum tropospheric photon energy of 400 kJ/mol although, 180 with the exception of formaldehyde (Moortgat et al., 1983), CO–loss QYs are low. For example, they are measured to be $\sim$0.02 in acetaldehyde (Blacet et al., 1942) and $\sim$0.01 for butanal (Blacet and Calvert, 1951).

The thresholds for roaming decarbonylation reactions are linked to the S_0 NTI asymptotic energies (Andrews et al., 2013; Mauguière et al., 2015; Bowman and Houston, 2017). For example, the roaming threshold in formaldehyde is $\sim$2 kJ/mol below the radical dissociation threshold (Townsend et al., 2004; Quinn et al., 2017), and both H and CH$_3$ roaming has been 185 observed in acetaldehyde (Lee et al., 2014). As such, the majority of aldehydes in the dataset have roaming thresholds that are similar to or lower in energy than the TS decarbonylation threshold, with formaldehyde a notable exception. Roaming
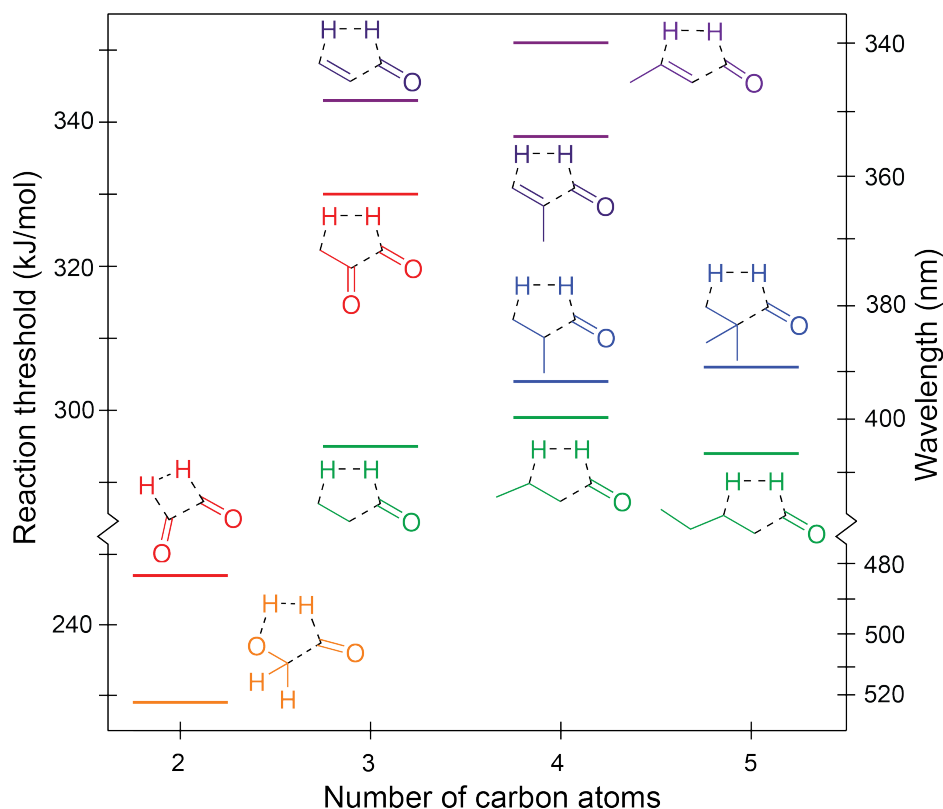
Figure 5. Zero-point vibrational energy corrected B2GP-PLYP-D3/def2-TZVP S_0 concerted triple fragmentation thresholds.

pathways associated with NTI may also be present in ketones (Goncharov et al., 2008; Saheb and Zokaie, 2018). This suggests decarbonylation will be energetically accessible under tropospheric conditions for all carbonyls.

3.2 Triple fragmentation (TF)

190 We define the TF reaction as a concerted S_0 reaction forming three products via a single TS, where one of these products is H_2. For example, the TF reaction in the saturated aldehyde propanal is: CH_3–CH_2–$(C=O)H \rightarrow H_2C=CH_2 + H_2 + CO$. For enals, the hydrocarbon product will be an alkyne. In dicarbonyls, TF forms H_2, CO, and either a second CO or ketene. Predicted S_0 TF thresholds are shown in Fig. 5. All of the TF reactions shown, except that for glyoxal, involve a 5-centre TS and H-loss from a β-hydrogen. In glyoxal, the 4-centre TS involves the two formyl hydrogens. The TSs are shown explicitly in Fig. S4 of

195 the Supplementary Material, and are 'late', resembling the photolysis products. As a result, TF threshold energies are strongly influenced by the stability of the products.

The TF thresholds for the saturated aldehydes are not significantly affected by chain extension, with thresholds of: 295, 299, and 294 kJ/mol for propanal, butanal, and pentanal, respectively. The effect of alkyl branching at the α-position is inconsistent and small. It raises the thresholds to 304 kJ/mol for 2-methylpropanal and 306 kJ/mol for 2,2-dimethylpropanal, but lowers

10

it for methacrolein (338 kJ/mol) compared to acrolein (343 kJ/mol). These differences are close to the likely accuracy of the B2GP-PLYP-D3 calculations.

The TF thresholds of the enals are significantly higher than those of the saturated aldehydes, at $\sim$340–350 kJ/mol. This increase is larger than the $\sim$10 kJ/mol increase seen in decarbonylation thresholds for breaking a delocalised C–C bond and arises because of bond angle strain in the 5-centre TF TSs of the α,β unsaturated species. As shown in Fig. S4, the C–C–C backbone angles in the TSs deviate significantly from their equilibrium values and the energetic penalty is increased, relative to saturated species, because of the rigidity of the delocalised C–C bonds.

The predicted S_0 TF thresholds of the two α-dicarbonyls, glyoxal and methylglyoxal, differ markedly, by 83 kJ/mol. This arises because their TS structures and reaction products are qualitatively different (Figs S4j and S4k). Methylglyoxal has a 5-centre TS that involves strain across the O=C–C=O backbone and also forms a relatively high energy ketene product. Glyoxal, in contrast, forms exothermically favourable products: H_2 and two CO molecules, resulting in a significantly lower S_0 TF threshold.

Glycolaldehyde is an atypical carbonyl and has the lowest energy TF pathway, calculated at 229 kJ/mol. Here, the H_2–loss channel arises from combination of the formyl-hydrogen and the OH-hydrogen, which is more labile than the backbone C–H hydrogens. The C–OH angle in the glycolaldehyde TS also involves minimal ring strain (Fig. S4l). This pathway has not been previously proposed for glycolaldehyde (Wallington et al., 2018; Bacher et al., 2001; Zhu and Zhu, 2010; Cui and Fang, 2011; So et al., 2015) and occurs via a 5-centre TS, which is lower in energy than the 4-centre TF TS for H_2 formation from the formyl and a β CH$_2$ hydrogen. Indeed it is the lowest energy dissociation pathway we have found in gylcolaldehyde.

3.3 Norrish Type III β-H transfer reaction (NTIII)

Alongside the Norrish Type I and II reactions, the lesser known 'Norrish Type III' reaction (NTIII) was proposed by Zahra and Noyes (1965) to explain the observation of acetaldehyde and propene as products of 3-methylbutan-2-one photoexcitation. NTIII involves a 4-centre TS, with β-hydrogen transfer from the backbone to the carbonyl moiety leading to formation of an aldehyde and an alkene, for example, RCH$_2$CH$_2$(C=O)R$' \rightarrow$ R–CH=CH$_2$ + H(C=O)R$'$. Experimentally, NTIII has been found to be a minor channel (Zahra and Noyes, 1965). However, since the alkene product from NTIII can also be formed in other S_0 reactions (TF, H_2-loss), NTIII needs to be well understood to disambiguate these mechanisms.

Figure 6 shows our calculated NTIII thresholds. These vary across a large energy range, from 310–417 kJ/mol. In glyoxal, methylglyoxal, and methyl vinyl ketone the NTIII thresholds are at or above the actinic maximum energy of 400 kJ/mol. The NTIII thresholds of the other α,β-unsaturated carbonyls lie between 380 and 400 kJ/mol. The high thresholds arise from resonance stabilisation of the breaking C–C bond and suggest NTIII is unlikely to be important in these species under tropospheric conditions.

The saturated carbonyls in Fig. 6 have NTIII thresholds in the range 310–355 kJ/mol. The NTIII thresholds decrease significantly when the main alkyl chain is lengthened past the β-position: there is a 38 kJ/mol lowering of the NTIII threshold from butanone to pentan-2-one, and a 21 kJ/mol lowering from propanal to butanal. The effect of alkyl chain lengthening beyond the β-position is also present in α,β-unsaturated carbonyls, although it is smaller, with only a 7 kJ/mol decrease in threshold from
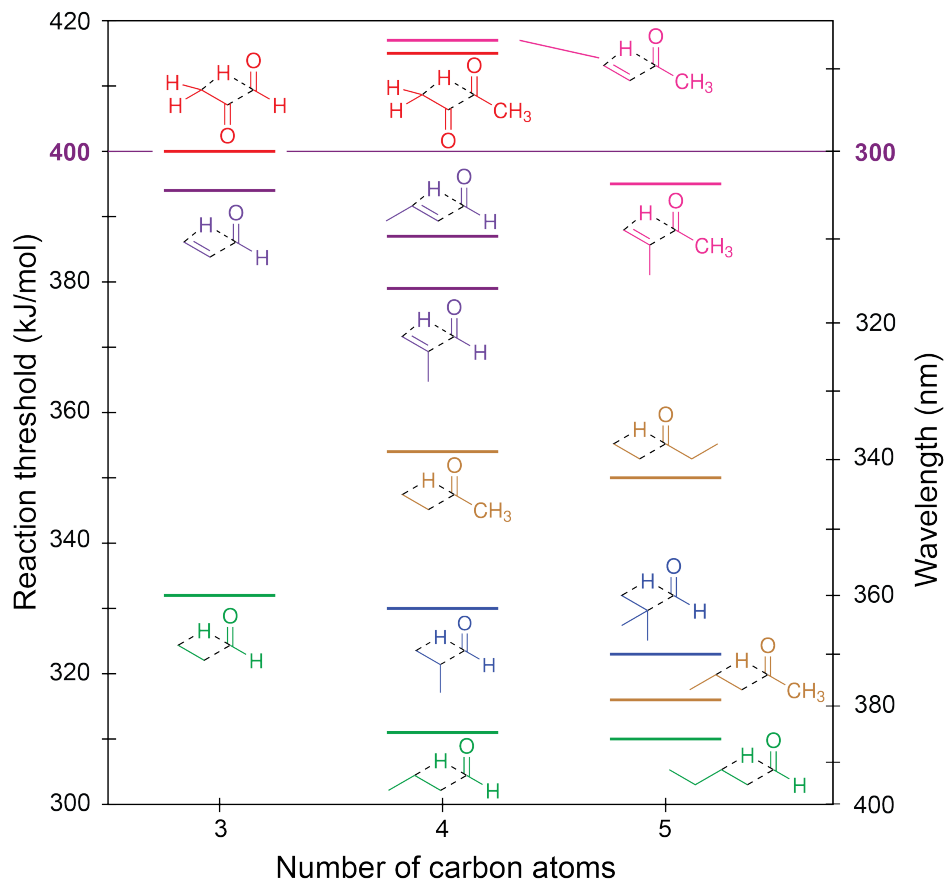
Figure 6. Zero-point vibrational energy corrected B2GP-PLYP-D3/def2-TZVP S_0 Norrish Type III thresholds.

acrolein to crotonaldehyde. The NTIII threshold, however, is unchanged with further alkyl chain lengthening. For example,

235   butanal and pentanal have almost the same NTIII threshold (311 and 310 kJ/mol respectively), and there is only a 4 kJ/mol difference in threshold between butanone and pentan-3-one. This suggests chain lengthening past the γ-position will not result in any change to the reaction threshold. The NTIII threshold also appears to be independent of the 'spectator' alkyl substituent in the ketones.

      Branching at the α-position decreases the NTIII threshold, though to a lesser extent than addition of a γ-carbon. The de-

240   creases are: 2 kJ/mol from propanal to 2-methylpropanal, 7 kJ/mol from 2-methylpropanal to 2,2-dimethylpropanal, 15 kJ/mol from acrolein to methacrolein, and 23 kJ/mol ketone to methyl isopropenyl ketone. These decreases in threshold energy exceed the expected uncertainty of our B2GP-PLYP-D3 calculations, except for the smallest 2 kJ/mol energy difference. The trends in NTIII threshold with both alkyl chain length and branching can be rationalised in terms of the alkene product formed: the relative stability of the alkene increases with increasing substitution about the double bond (Whangbo and Stewart, 1982).

3.4 Concerted 4-centre H_2–loss

H_2 can be formed on S_0 via a 4-centre TS where adjacent hydrogen atoms form an H–H bond and dissociate as H_2, leaving an unsaturated carbonyl product. In aldehydes these adjacent hydrogens can be the formyl and α hydrogens, but as the alkyl chain lengthens possibilities include hydrogens in the: $\alpha+\beta$, $\beta+\gamma$, etc., positions. These H_2–loss mechanisms can be distinguished by the point of unsaturation in the co-product.

The S_0 reaction thresholds for the possible H_2–loss channels are given in Table 1 and are shown in Fig. 7, where solid lines denote H_2–loss from the formyl and α positions; dashed lines, H_2–loss from the α and β positions; and dot-dashed lines, H_2–loss from the β and γ positions. Note that the y-axis of Fig. 7 is broken into three energy sections to indicate energetic separation between the different mechanisms.

Figure 7 indicates that thresholds for H_2–loss from the α and β positions are higher than from the formyl and α positions, with H_2–loss thresholds from the β and γ positions higher still. For a given carbonyl, the highest H_2–loss threshold is predicted for removal of a hydrogen from the terminal carbon. Like the NTIII reaction, the TSs for 4-centre H_2–loss are 'late', and the threshold energies are related to the stability of the forming alkene product. Increasing substitution around the double-bond increases alkene stability (Whangbo and Stewart, 1982), so products with a terminal C=C bond are comparatively less stable than products from H_2–loss at other sites. For example, there is an approximately 20 kJ/mol decrease in threshold for formyl + α H_2–loss from acetaldehyde to propanal. Like NTIII, there is little effect on the formyl and α H_2–loss threshold upon further chain extension. For example, the formyl and α H_2–loss thresholds for propanal, butanal and pentanal are all $\sim$315 kJ/mol. Branching at the α position also has little effect on the formyl and α H_2–loss threshold (*cf.* propanal and 2-methylpropanal). Similar trends are seen for H_2–loss from the α and β and β and γ positions.

The results in Table 1 and Fig. 7 reinforce, for multiple carbonyl species, that only H_2–loss from the formyl and α positions is energetically accessible in the actinic energy range. Indeed, the 4-centre H_2–loss channel in acetaldehyde has recently been observed experimentally under tropospherically relevant conditions (Harrison et al., 2019). In the absence of a formyl hydrogen, none of the ketone H_2–loss channels are accessible in the troposphere. Similarly, H_2–loss is not accessible in species lacking an α-hydrogen, like 2,2-dimethylbutanal and methacrolein.

The thresholds for H_2–loss from the formyl and α positions in acrolein and crotonaldehyde are also in the actinic range, at 373 and 386 kJ/mol, respectively. These thresholds are significantly higher than those for the saturated aldehydes because of the high energy of the product propadienone and 1,2-butadienone species and are close to the maximum actinic energy, suggesting S_0 H_2–loss is unlikely to be important in α,β-unsaturated aldehydes.

Glycolaldehyde is calculated to have the lowest H_2–loss threshold, 292 kJ/mol, for loss of the formyl and α hydrogens. This can be rationalised in terms of the electron withdrawing nature of the OH stabilising the 4-centre TS and the hydroxyketene product. Glyolaldehdye is also the only carbonyl with an energetically accessible β-H loss channel. Loss of the OH and β hydrogen forms glyoxal and H_2 with a 384 kJ/mol threshold, close to the actinic maximum energy.

3.5 Alkane/alkene elimination (AE)

In ketones, migration of an α-H atom to the 'other' α carbon via a 4-centre TS can form an alkane and a ketene. For example, acetone can dissociate to methane and ketene. In methyl vinyl ketone, the unsaturation leads to alkene elimination and formation of ethene and ketene.

The S_0 reaction thresholds for the lowest energy AE channels are given in Table 1 and are shown in Fig. 8. In asymmetric ketones two AE channels are possible and these are described in Sect. S6 of the Supplementary Material.

Figure 8 shows our calculated AE thresholds vary from 329 to 363 kJ/mol, with all accessible under tropospheric conditions. The TSs for AE are shown in Fig. S6.

In linear unsaturated ketones, the AE TSs are 'late', with C–C breaking bond lengths over 1.8 Å. Naïvely, we would therefore infer AE thresholds for these species will reflect the relative stability of the forming products. From tabulated 0 K enthalpies of formation (Ruscic et al., 2005; Ruscic, B. and Bross, D. H., 2020), although methyl ketene is 9 kJ/mol more stable than ketene, butanone is 17 kJ/mol more stable than acetone. This would imply a lower AE threshold in acetone. The AE threshold in butanone, however, is calculated to be 12 kJ/mol lower than that for acetone. The TS for AE in butanone (Fig. S6b) is marginally earlier than in acetone (Fig. S6a), suggesting electronic effects are responsible for the lower threshold. Only a 4 kJ/mol decrease in threshold, to 347 kJ/mol, is seen for production of ethylketene in pentan-2-one, indicating further chain lengthening has little effect. This threshold is the same as that calculated for pentan-3-one forming ethane and methylketene, that is, there is a small reduction in threshold energy on formation of a larger alkane. This is also seen in the alternate AE pathways (Sect. S6). As shown in Fig. S6, in linear unsaturated ketones, thresholds for producing ketene (via the alternate AE channels) are ~360 kJ/mol and thresholds for producing methylketene are ~350 kJ/mol. We expect these thresholds to be generalisable to larger linear unsaturated ketones.

The lowest AE thresholds are for methyl vinyl ketone and methyl isopropenyl ketone (MIPK), both of which yield ketene. The AE TSs in these molecules are much 'tighter' than in the linear unsaturated ketones (Fig. S6). Here there is resonance stabilisation of the saddle points, leading to thresholds of 329 and 334 kJ/mol, respectively.

3.6 Keto–enol tautomerisation

Carbonyls can exist in two tautomeric forms: a keto form (encompassing, here, both ketones and aldehydes), and an enol form where an H atom has transferred to the carbonyl oxygen, forming an OH substituent and a point of unsaturation. Keto–enol tautomerisation is known to occur as a dynamic equilibrium in S_0 carbonyls in aqueous solution at room temperature, although the keto tautomer is thermodynamically favoured (Keeffe et al., 1988). Keto–enol tautomerisation has been observed in gas phase photolysis experiments on acetaldehyde (Clubb et al., 2012; Shaw et al., 2018) and the authors suggest it may occur in many other carbonyls under tropospheric conditions. In solution or at higher gas pressures, keto-enol isomerisation is also readily catalysed by species containing acidic hydrogens – including water, alcohols, and organic and inorganic acids.

The lowest energy calculated keto–enol tautomerisation thresholds for the relevant carbonyls in the dataset are given in Table 1 and shown in Fig. 9. A keto–enol TS involving an α hydrogen, that is, a [1,2]-H atom shift, was found in all of these species.

In crotonaldehyde, however, the lowest energy threshold, 133 kJ/mol, was for a [1,5]-H atom shift involving a γ hydrogen and this is less than half the 294 kJ/mol threshold we predict for a [1,2]-H atom shift. This mechanism is analogous to the [1,5]-H atom shift in the Norrish Type II reaction. Here, however, because it occurs in an enal, conjugation prevents the bond between the α- and β-carbons from breaking and, instead, but-1,3-diene-1-ol, is formed.

There may be multiple possible [1,2]-H atom shift keto–enol tautomerisation pathways for a given carbonyl. These correspond to formation of geometric isomers (e.g. *cis*- or *trans*-enols) or, in asymmetric ketones, tautomerisation involving hydrogens from either alkyl substituent. These additional keto–enol tautomerisation thresholds are reported in Table S7 and all optimised saddle point geometries are shown in Fig. S7 of the Supplementary Material. As described in more detail in Sect. S7, due to steric factors, thresholds for tautomerisation to *trans*-enols are typically ~20 kJ/mol lower than those to the corresponding *cis*-enol.

As shown in Fig. 9, the keto–enol tautomerisation thresholds for linear aldehydes lie in a narrow energy range (278–281 kJ/mol), indicating chain extension has no effect on threshold as long as the bulky alkyl group can be oriented *trans* to the enol OH group. This is not the case for the α-branched 2-methylpropanal, and the steric penalty leads to the highest keto–enol tautomerisation threshold calculated here (296 kJ/mol).

The tautomerisation thresholds for ketones are also in a narrow range (270–276 kJ/mol), ~5 kJ/mol lower than the corresponding aldehydes. As shown in Table S7 this extends to the alternate pathway in asymmetrically substituted ketones, which have thresholds for formation of the alternate *trans*-enol within ~1 kJ/mol of those shown in Fig. 9.

In α,β-unsaturated carbonyls, the keto–enol tautomerisation thresholds are low when tautomerisation involves a H-atom from an aliphatic group, for example, the CH_3 group in methyl vinyl ketone and crotonaldehyde. Tautomerisation thresholds involving olefinc H-atoms, however, are significantly higher, for example 292 kJ/mol in acrolein, reflecting the relatively unstable propadienol product.

Glycolaldehyde has an –OH electron withdrawing functional group. For this molecule the tautomerisation threshold is predicted to be lowered by 8 kJ/mol compared to acetaldehyde, that is, the electron withdrawing group stabilises the TS to the forming enol.

Notably, all calculated keto–enol tautomerisation thresholds are significantly below the maximum actinic photon energy. We expect this pathway to be energetically accessible in all carbonyls with an α hydrogen and appropriate unsaturated species with a γ hydrogen. Moreover, all linear aldehydes and ketones are calculated to have keto–enol tautomerisation thresholds close to, or below, that of acetaldehyde. Given the experimental observation of keto–enol tautomerisation in acetaldehyde (Clubb et al., 2012; Shaw et al., 2018) and in acetone and methyl vinyl ketone (Couch et al., 2021), this tautomerisation may be important under tropospheric conditions in these species.

3.7 Enal–ketene tautomerisation

There has been recent interest in the formation of ketenes as atypical and relatively uncharacterised products of carbonyl photolysis (Harrison et al., 2019; Toulson et al., 2018). As seen above, the formyl + α H_2–loss mechanism forms ketenes in aldehydes and the AE mechanism forms ketenes in ketones. In enals there is also an S_0 tautomerisation mechanism involving

a [1,3]-H shift of the formyl-hydrogen to the β-carbon that can form ketenes. First order saddle points have been optimised for enal–ketene tautomerisation in acrolein, crotonaldehyde and methacrolein. These are shown in Fig. 10, together with the calculated B2GP-PLYP-D3 threshold energies. The enal–ketene tautomerisation threshold in methacrolein, 285 kJ/mol, is $\sim$14 kJ/mol lower in energy than the 299 kJ/mol G3X-K//M06-2X/6-31G(2df,p) threshold previously calculated by So et al. (2018). This difference is consistent with the variation between B2GP-PLYP-D3 and G3X-K thresholds for other reactions considered in methacrolein and methyl vinyl ketone (see Supplementary Material) and may be due to the treatment of dispersion in the saddle point geometries.

Figure 10 shows the key structural parameters describing the TSs for S_0 enal–ketene tautomerisation are almost identical for the three enals in the dataset. This indicates α-branching and main alkyl chain extension have negligible effect on the TS geometry and little effect on the threshold energy. The predicted enal–ketene tautomerisation thresholds are all well below the maximum actinic energy of 400 kJ/mol and suggest that, in appropriate species, enal–ketene tautomerisation may be competitive in the troposphere.

4   Competition between carbonyl S_0 reactions

Our calculated S_0 thresholds can be compared to relevant experimental results, to validate the calculations, generalise our results and to predict the most important S_0 reactions for each class of carbonyl. Indeed, the seven reaction thresholds depicted for butanal in Fig. S1 are illustrative of the energetic relevance of these channels in other saturated aldehydes.

4.1   Saturated aldehydes

For saturated aldehydes, the lowest energy dissociation pathway on S_0 is concerted TF, with a threshold of $\sim$300 kJ/mol. At wavelengths and internal energies where excited state chemistry is energetically inaccessible, TF may therefore be a significant photo-induced mechanism. Triple fragmentation has been observed as a primary photolysis mechanism in propanal and 2-methylpropanal, with QYs of 4% and 9%, respectively, at 1 atm pressure of N_2 (Kharazmi, 2019). On the basis of kinetic modelling and, in the absence of excited state primary pathways, both sets of TF products were found to be consistent with S_0 reaction. The increased QY for 2-methylpropanal over propanal was attributed to increased reaction path degeneracy rather than a lower reaction threshold. This suggests TF QYs will be higher in branched aldehydes, in proportion to the ratio of β-hydrogens. For example, we predict 2,2-dimethylpropanal, with nine β-hydrogens to have a higher TF QY than 2-methylpropanal, with six β-hydrogens, and propanal, with three β-hydrogens.

The next lowest energy S_0 dissociation pathway is either H_2-loss from the formyl and α–H atoms in the smaller species (acetaldehyde, propanal, methylpropanal) or NTIII in the larger species (butanal, pentanal, 2,2-dimethylpropanal). For formyl + α H_2-loss, acetaldehyde has three α hydrogens and the highest threshold at 337 kJ/mol. This channel has been observed experimentally, with a QY of $\sim$1% at 305 nm (392 kJ/mol) and 1 atm of N_2 and is demonstrated to be a primary process by single molecule velocity map ion-imaging (VMI) experiments (Harrison et al., 2019). Although classical trajectory simulations initiated at the H_2-loss TS could not reproduce the VMI product state distributions, they are consistent with an S_0

roaming mechanism (Harrison et al., 2019). The equivalent H_2-loss thresholds for the other saturated aldehydes, which have two rather than three α hydrogen atoms, are significantly lower, at ~315 kJ/mol. Thus we expect H_2–loss reactions to be present in other saturated aldehydes with similar, or slightly higher QYs than in acetaldehyde. Indeed, under tropospheric conditions, methylketene and dimethylketene have been observed as minor products following photolysis of propanal and 2-methylpropanal, respectively, with kinetic modelling consistent with S_0 reaction (Kharazmi, 2019). In saturated aldehydes, the NTIII thresholds are similar to those for H_2–loss. Experimental QYs for this pathway, however, have not been reported. The NTIII mechanism shares common products with TF (alkene) and decarbonylation (CO), which may complicate its experimental identification. Our calculations suggest NTIII is energetically competitive, and it may be important in interpreting photolysis QYs of saturated aldehydes.

With the exception of formaldehyde, the next lowest energy S_0 dissociation threshold is for ground state NTIa, that is, α-bond cleavage to the alkyl substituent. This reaction is typically assumed to occur only on T_1 but the S_0 reaction has been identified in formaldehyde (Quinn et al., 2017), acetaldehyde (Heazlewood et al., 2009; Amaral et al., 2010) and acetone (Lee et al., 2017). Because it is barrierless we expect S_0 NTIa to dominate as internal energy increases above its threshold. Thus, we expect to observe NTIa dissociation products at energies well below the T_1 threshold.

Decarbonylation (CO–loss) has the highest calculated S_0 dissociation thresholds for all the saturated carbonyls in the dataset, bar formaldehyde, for which the decarbonylation threshold is slightly below that of NTI. All decarbonylation thresholds are predicted to be 340–350 kJ/mol and experimental CO–loss QYs are correspondingly low: in the actinic energy range, the atmospheric pressure decarbonylation QY for acetaldehyde is ~0.5% (Moortgat et al., 2010; Warneck and Moortgat, 2012) and ~0.2% for 2-methylbutanal (Gruver and Calvert, 1958). Although two S_0 decarbonylation mechanisms are known, roaming reactions and reaction via a TS, there is no known excited state decarbonylaiton mechanism. Given the relatively high threshold energies, we predict other S_0 pathways will be favoured in larger saturated aldehydes over decarbonylation, which will be at most a minor channel.

Our calculations predict keto–enol tautomerisation to be the lowest energy pathway on S_0 for all saturated aldehydes, lying about 20 kJ/mol below TF. Unlike dissociation, however, tautomerisation is reversible. Collisional cooling into the enol well therefore competes with tautomerisation back to the parent aldehyde (Andrews et al., 2012). Dissociation of the aldehyde reduces its concentration and hence, while the rate coefficient is constant, the rate of enol formation is reduced. Although experimentally observed in ketones, the only aldehyde for which photo-initiated keto–enol tautomerisation has been observed is acetaldehyde (Clubb et al., 2012; Shaw et al., 2018), where TF is not available and master equation modelling confirms that it is an S_0 process Shaw et al. (2018). Whilst it is likely keto–enol tautomerisation is occurring in other saturated aldehydes, QYs are likely small and the reactivity of the enol will make characterisation difficult.

4.2 Saturated ketones

Following excitation by an actinic photon, the relevant S_0 chemistry of ketones is much simpler than that of aldehydes. No TS for direct decarbonylation was found and the absence of a formyl H–atom in ketones removes the TF and formyl + α H_2–loss pathways. The only S_0 dissociation pathways in ketones are NTIII, AE and NTI. The thresholds for AE and NTI are similar

410   in the ketones considered, at ~340 kJ/mol. Given NTI is barrierless, it is likely to dominate over AE. We therefore expect NTI to be the dominant dissociation mechanism in acetone, butanone and pentan-2-one, where it has a lower threshold than NTIII, although NTIII may be important in pentan-2-one and in larger saturated ketones, where there is alkyl chain extension past the β-hydrogen involved in the reaction. For example, the production of acetaldehyde from 3-methylbutan-2-one is one of the few experimental examples of the, assumed S_0, NTIII mechanism in the literature (Zahra and Noyes, 1965).

415   The keto–enol tautomerisation thresholds for saturated ketones are slightly lower than in saturated aldehydes. This, combined with the absence of low energy S_0 dissociation pathways and the experimental observation of keto–enol tautomerisation in acetone under thermal conditions, where reaction must occur on S_0 (Couch et al., 2021), suggests photo-initiated tautomerisation may be important in ketones.

4.3 α,β-Unsaturated carbonyls

420   In general, because of resonance stabilisation of the bond between α- and formyl-carbons, we calculate higher S_0 thresholds in α,β-unsaturated carbonyls than in equivalent saturated carbonyls. However, excited state NTIa thresholds are also elevated and all excited state NTI thresholds are close to, or above, the maximum available actinic energy (Rowell et al., 2019). Thus any photolysis must occur on S_0. Further, unlike many other carbonyls, the electronic structure of the α,β-unsaturated carbonyls promotes rapid electronic relaxation from S_1 to S_0 (Lee et al., 2007; Schalk et al., 2014; Cao and Xie, 2016), suggesting high
425   S_0 internal energies and therefore relatively high probability of S_0 reaction.

   Triple fragmentation is the lowest energy S_0 dissociation pathway for the unsaturated aldehydes in the dataset. The TF thresholds are ~40 kJ/mol higher than in saturated aldehydes and are slightly lower than the S_0 NTIb asymptotic energies and decarbonylation thresholds. The other possible S_0 dissociation reactions (H$_2$-loss, NTIII and S_0 NTIa) have thresholds >370 kJ/mol and are unlikely to be significant under tropospheric conditions.

430   Unsaturated ketones, like their saturated counterparts, have fewer S_0 dissociation pathways, with only NTIII, AE, NTIa and NTIb possible. In methyl vinyl ketone, AE has the lowest threshold, at 329 kJ/mol, 9 kJ/mol lower than the NTIb threshold. NTIb dissociation, however, is barrierless. The 334 kJ/mol threshold for AE is the lowest energy S_0 pathway in methyl isopropenyl ketone, 10 kJ/mol lower than the threshold for NTIb dissociation. Although NTIb will dominate at higher energies, there may be a small energy window where AE may be important, although it has not been experimentally observed. Similarly,
435   there may be an energy window for AE in methyl vinyl ketone. The other possible dissociations in methyl vinyl ketone, NTIa and NTIII, have thresholds >375 kJ/mol and are unlikely to be important under tropospheric conditions.

   Given the lack of low energy ground or excited state dissociation pathways, we expect photolysis QYs for α,β-unsaturated carbonyls to be small. Indeed the total photolysis QY of methacrolein is around 1% at atmospheric pressure (Raber and Moortgat, 1996). Photo-induced keto–enol and enal–ketene tautomerisations, however, have thresholds under 300 kJ/mol, with
440   crotonaldehyde having a lowest energy keto–enol tautomerisation threshold of 133 kJ/mol. Tautomerisation has been observed in methyl vinyl ketone under thermal conditions (Couch et al., 2021), and S_0 tautomerisation may therefore be competitive for appropriate α,β-unsaturated species (So et al., 2018). The higher energy enol and ketene isomers may be collisionally

stabilised under tropospheric conditions, although they are significantly more reactive and will be difficult to experimentally isolate.

4.4 Other carbonyls

The α-dicarbonyls have low energy π_+^* excited states (Arnett et al., 1974; Dykstra and Schaefer, 1976), red-shifted absorption spectra compared to other carbonyls (Fig. 1) and weakened α-C–C bonds due to the electron withdrawing nature of the two C=O chromophores. As a result, the excited state NTIa thresholds in dicarbonyls are lowered to $\sim$390 kJ/mol on S_1 and $\sim$300 kJ/mol on T_1 (Rowell et al., 2019), with both accessible in the troposphere. The S_0 asymptotic energies for NTIa are slightly lower than the triplet thresholds, giving an energetic window for S_0 radical dissociation. Indeed, in glyoxal, two distinct, wavelength-dependent mechanisms of HCO$^\bullet$ formation have been observed and attributed to dissociation on two electronic states (Chen and Zhu, 2003; Kao et al., 2004; Salter et al., 2013). Decarbonylation to form H_2CO + CO and TF to form H_2 + 2 CO have the lowest energy thresholds in glyoxal, at 225 and 247 kJ/mol, respectively. Indeed, CO is known to form following irradiation of glyoxal at energies below 272 kJ/mol (Loge and Parmenter, 1981; Hepburn et al., 1983; Burak et al., 1987; Dobeck et al., 1999). Decarbonylation in methylglyoxal also has a low threshold energy, 235 kJ/mol, and we expect it to be the dominant S_0 dissociation mechanism. In diacetyl, without a formyl hydrogen, NTIa has the lowest dissociation threshold. We therefore predict, for larger α-dicarbonyls, there will be an actinic window from $\sim$300–266 kJ/mol with no accessible dissociation pathways. In this case, collisional cooling and thermalisation to the parent carbonyl is the likely fate.

The remaining carbonyl in the dataset is glycolaldehyde, with an actinic range between 352 and 400 kJ/mol (Bacher et al., 2001). The NTIa thresholds on S_1 and T_1 for glycolaldehyde are 379 and 334 kJ/mol, respectively (Rowell et al., 2019), and this channel dominates at all actinic energies (Bacher et al., 2001; Zhu and Zhu, 2010), with cleavage of the C–OH bond to form $^\bullet$OH also reported (Zhu and Zhu, 2010). Thus, despite having the lowest calculated TF and H_2–loss thresholds, these reactions have not been experimentally observed in glycolaldehyde. Keto–enol tautomerisation to 1,2-ethenediol, for which we calculate a threshold of 272 kJ/mol, has been postulated as an atmospheric route to formation of $HO_2^\bullet$ and formic acid (So et al., 2015), although it has not been experimentally observed.

5 Tropospheric relevance of S_0 reactions

A few guiding principles can be used to determine which of the possible S_0 pathways may be tropospherically relevant in a given carbonyl following absorption of an actinic photon.

- Reactions with thresholds greater than the actinic maximum energy of 400 kJ/mol are inaccessible at tropospheric photon energies. This rules out most S_1 reactions, with exceptions of NTIa dissociation in glycolaldehyde and NTIb in methyl vinyl ketone and methyl isopropenyl ketone (Haas, 2004; Rowell et al., 2019). T_1 NTI dissociations *are* accessible. T_1 NTIb thresholds are close to the maximum available energy of 400 kJ/mol and have negligible contribution to actinic photolysis (Zhu et al., 2009), T_1 NTIa thresholds are generally lower (Rowell et al., 2019), and this reaction dominates the photolysis QY of small carbonyls (Kirkbride and Norrish, 1931; Zhu et al., 2009). In larger carbonyls (alkyl chains

475   lengths $\geq$ 4), excited state NTII intramolecular γ-H abstraction is also accessible (Wagner and Zepp, 1972; Wagner and Klán, 2004; Zhu et al., 2009).

- For photon energies above their thresholds, T_1 reactions are fast and dominate photolysis (Kirkbride and Norrish, 1931; Zhu et al., 2009). If the photon energy is near threshold, non-radiative transitions and S_0 reaction may be competitive with excited state reaction. For photon energies (or collisional cooling on S_1 or T_1) below any excited state threshold, any photolysis must occur on S_0. There is significant overlap of the absorption spectrum of most carbonyls with these lower energy photons (Fig. 1) and S_0 reactions have been observed in saturated carbonyls under these conditions (Heazlewood et al., 2009; Amaral et al., 2010; Andrews et al., 2012; Tsai et al., 2015; Quinn et al., 2017; Toulson et al., 2018).

- For an S_0 process to be tropospherically important, its rate must be competitive with collisional cooling and thermal equilibrium. Only S_0 dissociations with thresholds <350 kJ/mol have been experimentally observed following photoexcitation of aldehydes in 1 atm of N_2 (Clubb et al., 2012; Shaw et al., 2018; Harrison et al., 2019). Because of the efficiency of collisional cooling, the most important S_0 dissociations are likely to be those with the lowest thresholds, that is, TF if available, NTI in ketones and selected AE, NTIII and formyl+α H_2–loss reactions.

- Although S_0 keto–enol and enal–ketene tautomerisations have the lowest calculated thresholds, these are reversible reactions where collisional stabilisation of the tautomer competes with isomerisation back to and dissociation of the parent carbonyl. Tautomerisation, per se, is therefore unlikely to be important if there are low energy S_0 dissociation pathways. It will be important in the absence of such a channel, for example, in acetaldehyde (Clubb et al., 2012; Shaw et al., 2018), some ketones and some α,β-unsaturated carbonyls. Tautomerisation may also have an indirect effect on other S_0 reactions. Rapid interconversion of tautomers will reduce the effective concentration of the 'keto' form and hence reduce the probability of other possible S_0 reactions.

495   The atmospheric importance of photo-initiated S_0 reactions is as yet unknown, however, S_0 reactions are likely to be broadly accessible under tropospheric conditions for all carbonyls. They are therefore likely in regions of the troposphere with high carbonyl concentrations: in highly polluted environments, where carbonyls are both directly emitted and are oxidation products of other VOCs, and in unpolluted, forested environments, where oxidation of BVOCs leads to unsaturated carbonyls like methacrolein and methyl vinyl ketone (Kesselmeier and Staudt, 1999; Millet et al., 2010; Chen et al., 2014). Carbonyls are also important species in the marine boundary layer, although there are significant discrepancies between observed and modelled concentrations (Vigouroux et al., 2009; Anderson et al., 2017; Ahn et al., 2019).

    Photo-initiated S_0 reactions of carbonyls have a number of atmospheric consequences. The majority of reactions lead to molecular, rather than radical, products and this may effect modelled radical quantum yields and therefore radical propagation reactions. Many of the S_0 reaction products are also 'unexpected', and form unsaturated species such as alkenes, alkynes, enols and ketenes that are more reactive than their parent carbonyl, particularly to addition reactions, for example, with $^\bullet$OH and NOx radicals and even atmospheric H_2O (Atkinson et al., 2006; So et al., 2014; Kahan et al., 2013). We suggest ground state

reactions should be considered whenever unexpected products are found in the laboratory photolysis of carbonyls and when products are observed following photolysis below excited state thresholds.

The experimental observations of photo-initiated S_0 reactions in carbonyls described in this paper indicate the parent carbonyl is returning to the ground electronic state with energies close to the original photon energy. In addition to dissociation and isomerisation, these vibrationally 'hot' S_0 molecules could also react with other atmospheric species: their high internal energy makes otherwise inaccessible reactions energetically feasible. For example, internally excited carbonyls could undergo rapid bimolecular reaction with species such as O_2, H_2O, $^{\bullet}OH$, NOx and NH_3. The possibility of a reaction between O_2 and internally hot acetaldehyde, formed following excitation at 248 nm, considerably above the actinic range, was speculated by Morajkar et al. (2014), although this was not further investigated or resolved. Such bimolecular reactions may lead to radical species and we suggest they may be responsible for radical QYs observed following photolysis at energies below the NTI thresholds in formaldehyde (Horowitz and Calvert, 1978; Moortgat and Warneck, 1979; Valachovic et al., 2000). In this sense, whilst the *total* experimental radical QY may be correct, the reaction mechanism is not simply unimolecular dissociation and radical QYs from bimolecular reaction will have different pressure dependence to those from unimolecular dissociation.

The molecular products of some of the S_0 reactions considered are also formed with extremely high internal energy. Experimentally, the roaming pathway in formaldehyde forms H_2 with up to 12 quanta of vibrational excitation (Quinn et al., 2017). Similarly, CH_4 from roaming in acetaldehyde is formed with internal energies up to 95% of the CH bond dissociation energy (Heazlewood et al., 2008). Although its mechanism has not been elucidated, the formyl+α H_2-loss channel in acetaldehyde has been shown experimentally to yield internally hot ketene, with energy > 150 kJ/mol (Harrison et al., 2019). These 'hot' molecular products could also potentially undergo bimolecular reactions in the atmosphere and contribute toward radical QYs.

There are two cases where photo-initiated S_0 reactions of carbonyls have immediate tropospheric implications and missing or underestimated photochemical sources have previously been speculated. These are the formation of organic acids and the photolytic generation of molecular hydrogen, H_2. In both polluted and pristine regions there are discrepancies between the predictions of atmospheric models and field measurements of the concentrations of organic acids (Cady-Pereira et al., 2014; Yuan et al., 2015; Millet et al., 2015), although a recent paper by Franco et al. (2021) proposes a pathway that may close the gap. Depending on the type of model and the estimation of soil uptake, there are also large differences in estimates of global photochemical production of H_2 (Novelli, 1999; Rhee et al., 2006; Price et al., 2007; Xiao et al., 2007; Ehhalt and Rohrer, 2009; Yashiro et al., 2011; Patterson et al., 2020). Notably, in 'top-down' models, Rhee et al. (2006) and Xiao et al. (2007) propose increased H_2 production from photolysis of oxidized non-methane VOCs.

The tautomerisation of acetaldehyde to vinyl alcohol, addition of atmospheric $^{\bullet}OH$ and subsequent oxidation has been modelled and shown to produce significant global tropospheric formic acid and was found to be the dominant mechanism for formic acid formation in the marine boundary layer (Shaw et al., 2018). This one reaction, however, is not sufficient to explain the factor of two discrepancy between modelled and measured global organic acid concentrations (Shaw et al., 2018). Keto–enol isomerisation is present in almost all carbonyls we have considered, having amongst the lowest S_0 reaction thresholds. Similar reactions involving other unsaturated products, for example alkenes and ketenes (Atkinson et al., 2006; Kahan et al., 2013), will also lead to organic acid formation. We expect these reactions to be energetically accessible in most atmospheric

carbonyls and their cumulative effect may address the modelled deficit (Shaw et al., 2018; So et al., 2018). Understanding the mechanism of formation of organic acids in the troposphere has further application to secondary aerosol formation; the higher oxygen content of organic acids reduces their volatility and, as proton donors, they are believed to be key species in the nucleation and growth of atmospheric particles (Zhang et al., 2004; Bianchi et al., 2016; Tröstl et al., 2016; Liu et al., 2021).

Molecular hydrogen is an important atmospheric reducing agent and is an indirect greenhouse gas because it increases the atmospheric lifetime of CH_4 (Ehhalt and Rohrer, 2009). Current understanding indicates the major photochemical source of H_2 in the atmosphere is photolysis of formaldehyde, which accounts for at least half of the photochemically generated H_2 (Hauglustaine, 2002). The mechanisms generating the other half are unknown (Grant et al., 2010). The energetically accessible S_0 TF and/or H_2-loss reactions present in all aldehydes in our dataset, and expected in all atmospheric aldehydes, provide primary photolysis routes to H_2 that have not previously been considered. By better understanding the current atmospheric H_2 budget, we are better placed to model any future increase in atmospheric H_2, for example, due to leakage of H_2 in any transition to a hydrogen economy.

5.1 Challenges to address

To definitively answer the question 'how important is the photo-initiated ground state chemistry of carbonyls in the atmosphere?' a number of challenges need to be addressed. Experimentally these include observation of primary products formed on S_0 and characterisation of S_0 QYs. An understanding of the competition between collisional cooling and reaction under tropospheric conditions is also required.

Primary photolysis products can be observed in single molecule experiments, for example, Harrison et al. (2019) recently observed the formyl+α H_2-loss channel in acetaldehyde using velocity map ion-imaging. These experiments, however, do not provide absolute QYs. An additional challenge is that many of the products formed are either transient and difficult to observe under atmospheric conditions or can be formed from multiple reaction pathways. Determination of S_0 QYs therefore relies on master equation modelling and hence on an accurate characterisation of reaction mechanisms. The results in this paper are a necessary step toward such modelling and will inform the interpretation of photolysis experiments on individual carbonyls, box models of specific locations and ultimately global chemical transport models.

Very little is known about collisional cooling of highly excited ground state molecules. Modelling of experimental photolysis QYs of acetaldehyde, using a simple exponential-down model, suggests an average loss of 150 cm^{-1} ($\sim$1.8 kJ/mol) internal energy per collision with N_2 (Andrews et al., 2012). The accuracy of this model and the generality of this result to other carbonyls and their isomers are yet to be tested. Nevertheless, it suggests of the order of 200 collisions are required to thermalise carbonyls after absorption of an actinic photon. Given collision frequencies of the order of 10^9 s^{-1} at atmospheric pressure, unimolecular reactions with rate coefficients of magnitude 10^7 or more are likely to be competitive under tropospheric conditions. For example, for deuterated acetaldehyde following excitation by 322.9 nm light, Heazlewood et al. (2011) calculated unimolecular rate coefficients for S_0 NTI dissociation, decarbonylation, formyl+α H_2-loss and keto–enol tautomerisation of approximately 1×10^7, 1×10^6, 2×10^6, and 2×10^7 s^{-1}, respectively. There is experimental evidence for all of these S_0 reactions under tropospheric conditions (Heazlewood et al., 2009; Horowitz and Calvert, 1982; Heazlewood et al., 2008; Moortgat

et al., 2010; Harrison et al., 2019; Clubb et al., 2012; Shaw et al., 2018), although decarbonylation and formyl+α H$_2$-loss are minor channels. Many of the S_0 thresholds in Table 1 are lower than those for acetaldehyde, implying higher reaction rate coefficients, although these are yet to be calculated.

Meeting these challenges will enable the tropospheric importance of photo-initiated S_0 reactions in individual carbonyls to be determined. Even if these individual reactions have small QY, their presence in all atmospheric carbonyls may lead to cumulative products that may be atmospherically significant.

6   Conclusions

We have calculated S_0 reaction thresholds for nine reaction types in seven classes of carbonyl within a 'small' carbonyl dataset. In general, the S_0 transition states are 'late' and resemble the products. Reaction threshold energies typically correlate with the stability of the product molecules, enabling our results to be generalised to larger carbonyls.

In the smallest carbonyls and dicarbonyls, formaldehyde, glyoxal and methylglyoxal, the lowest energy threshold is for direct decarbonylation and this mechanism will compete with NTI dissociation. In larger aldehydes direct decarbonylation via a TS mechanism has a threshold of ∼350 kJ/mol in saturated species and ∼360–375 in α,β-unsaturated species. This reaction is therefore likely unimportant in larger aldehydes. However, alternate roaming pathways may be viable if there are low energy barrierless S_0 NTI pathways.

In larger carbonyls, the lowest energy S_0 dissociation thresholds are for triple fragmentation (TF) of both saturated (∼300 kJ/mol) and α,β-unsaturated (∼340 kJ/mol) aldehydes, with negligible impact from extension of the main alkyl chain. Branching at the α-position only increases TF thresholds by ∼5 kJ/mol, but increases the reaction path degeneracy and hence, likely, the QY.

The only 4-centre H$_2$-loss mechanism relevant at actinic energies involves the formyl and α hydrogens, and so need only be considered for aldehydes. This threshold is highest, at 337 kJ/mol, for acetaldehyde, and we expect it to be ∼315 in other aldehydes since a terminal double-bond is not being formed.

The NTIII β-hydrogen transfer reaction is energetically accessible in saturated carbonyls, but largely inaccessible for α,β-unsaturated species. This pathway is often overlooked in the interpretation of photolysis experiments but should be considered when the production of alkenes and aldehydes shows little-to-no pressure dependence.

We expect alkane elimination to have thresholds of ∼350 kJ/mol in linear unsaturated ketones. Whilst energetically accessible under tropospheric conditions, these thresholds are above those for NTI dissociation and we do not expect alkane elimination to be significant. The AE threshold, however, is reduced to ∼330 kJ/mol by branching or unsaturation at the α position and alkene elimination may be important in these species.

Finally, where present, tautomerisation pathways have the overall lowest S_0 thresholds and yield highly reactive unsaturated species: enols or ketenes. The keto–enol tautomerisation of acetaldehyde to vinyl alcohol leads to significant formation of formic acid in the troposphere. This process may be relevant to other atmospheric carbonyls. In particular, the α,β-unsaturated

carbonyls have UV absorption spectra that extend to low energies, high excited state reaction thresholds and relatively high S_0 dissociation thresholds.

610   The calculations in this paper demonstrate a range of ground state reactions are energetically accessible within the tropospheric "photochemistry" of carbonyls. The energetic thresholds for these S_0 reactions are some of the lowest calculated for any carbonyl reaction, on any electronic state. Many of the TF reactions as well as the keto–enol and enal–ketene tautomerisation are predicted to have reaction thresholds $\lesssim$300 kJ/mol. These reactions are likely to be important following photoexcitation at energies below any excited state reaction threshold or following collisional cooling of excited state carbonyl molecules below

615   such thresholds. An assessment of the likelihood of these S_0 reactions and determination of their product yields, however, requires calculation of the respective reaction rate coefficients and master equation modelling. Our results will help target such calculations, as well as future experimental efforts, to reactions most likely to have tropospheric consequences. It may also be that the QY for the S_0 reactions of an individual carbonyl is relatively small. The fact that one or more of these reactions are expected to occur in *all* atmospheric carbonyls suggests that, cumulatively, they may be significant in the troposphere and may

620   have atmospheric consequences.

Supplementary Material: The supplement related to this article contains a figure and discussion of the energetic thresholds for relevant S_0 reactions in butanal; For the reaction classes considered, excepting enal–ketene tautomerisation, a review of the previous computational literature, additional higher energy thresholds, as applicable, and representations of the optimised S_0 first-order saddle points (excepting those for H_2–loss); Cartesian coordinates for all optimised saddle points are provided as

625   text filed in a ZIP folder. https://doi.org/10.5194/acp-0-1-2021-supplement

Author contributions. K.N.R. performed all calculations and data analysis. M.J.T.J. and S.H.K. conceived and directed the project, M.J.T.J. supervised the calculations. All authors contributed to data interpretation and the drafting of the manuscript.

References

Ahn, D. H., Choi, T., Kim, J., Park, S. S., Lee, Y. G., Kim, S.-J., and Koo, J.-H.: Southern Hemisphere mid- and high-latitudinal AOD, CO, NO$_2$, and HCHO: Spatiotemporal patterns revealed by satellite observations, Prog. Earth Planet. Sci., 6, 34, https://doi.org/10.1186/s40645-019-0277-y, 2019.

Amaral, G. A., Arregui, A., Rubio-Lago, L., Rodríguez, J. D., and Baares, L.: Imaging the radical channel in acetaldehyde photodissociation: Competing mechanisms at energies close to the triplet exit barrier, J. Chem. Phys., 133, 064 303, https://doi.org/10.1063/1.3474993, 2010.

Anderson, D. C., Nicely, J. M., Wolfe, G. M., Hanisco, T. F., Salawitch, R. J., Canty, T. P., Dickerson, R. R., Apel, E. C., Baidar, S., Bannan, T. J., Blake, N. J., Chen, D., Dix, B., Fernandez, R. P., Hall, S. R., Hornbrook, R. S., Gregory Huey, L., Josse, B., Jöckel, P., Kinnison, D. E., Koenig, T. K., Le Breton, M., Marécal, V., Morgenstern, O., Oman, L. D., Pan, L. L., Percival, C., Plummer, D., Revell, L. E., Rozanov, E., Saiz-Lopez, A., Stenke, A., Sudo, K., Tilmes, S., Ullmann, K., Volkamer, R., Weinheimer, A. J., and Zeng, G.: Formaldehyde in the tropical Western Pacific: Chemical sources and sinks, convective transport, and representation in CAM-Chem and the CCMI models, J. Geophys. Res. Atmos., 122, 11 201–11 226, https://doi.org/10.1002/2016JD026121, 2017.

Andrews, D. U., Heazlewood, B. R., Maccarone, A. T., Conroy, T., Payne, R. J., Jordan, M. J. T., and Kable, S. H.: Photo-Tautomerization of acetaldehyde to vinyl alcohol: A potential route to tropospheric acids, Science, 337, 1203–1206, https://doi.org/10.1126/science.1220712, 2012.

Andrews, D. U., Kable, S. H., and Jordan, M. J.: A phase space theory for roaming reactions, J. Phys. Chem. A, 117, 7631–7642, https://doi.org/10.1021/jp405582z, 2013.

Arnett, J. F., Newkome, G., Mattice, W. L., and McGlynn, S. P.: Excited electronic states of the α-dicarbonyls, J. Am. Chem. Soc., 96, 4385–4392, https://doi.org/10.1021/ja00821a007, 1974.

Atkinson, R. and Arey, J.: Atmospheric degradation of volatile organic compounds, Chem. Rev., 103, 4605–4638, https://doi.org/10.1021/cr0206420, 2003.

Atkinson, R., Baulch, D., Cox, R., Hampson, R., Kerr, J., Troe, J., and Troe, J.: Evaluated kinetic and photochemical data for atmospheric chemistry: Supplement IV: IUPAC subcommittee on gas kinetic data evaluation for atmospheric chemistry, Atmos. Environ. A, 26, 1187–1230, https://doi.org/10.1016/0960-1686(92)90383-V, 1992.

Atkinson, R., Baulch, D., and Cox: Evaluated kinetic and photochemical data for atmospheric chemistry: Volume II – gas phase reactions of organic species, Atmos. Chem. Phys., 6, 3625–4055, https://doi.org/10.5194/acp-6-3625-2006, 2006.

Bacher, C., Tyndall, G. S., and Orlando, J. J.: The atmospheric chemistry of glycolaldehyde, J. Atmos. Chem., 39, 171–189, https://doi.org/10.1023/A:1010689706869, 2001.

Bey, I., Jacob, D. J., Yantosca, R. M., Logan, J. A., Field, B. D., Fiore, A. M., Li, Q., Liu, H. Y., Mickley, L. J., and Schultz, M. G.: Global modeling of tropospheric chemistry with assimilated meteorology: Model description and evaluation, J. Geophys. Res. Atmos., 106, 23 073–23 095, https://doi.org/https://doi.org/10.1029/2001JD000807, 2001.

Bianchi, F., Tröstl, J., Junninen, H., Frege, C., Henne, S., Hoyle, C. R., Molteni, U., Herrmann, E., Adamov, A., Bukowiecki, N., Chen, X., Duplissy, J., Gysel, M., Hutterli, M., Kangasluoma, J., Kontkanen, J., Kürten, A., Manninen, H. E., Münch, S., Peräkylä, O., Petäjä, T., Rondo, L., Williamson, C., Weingartner, E., Curtius, J., Worsnop, D. R., Kulmala, M., Dommen, J., and Baltensperger, U.: New particle formation in the free troposphere: A question of chemistry and timing, Science, 352, 1109–1112, https://doi.org/10.1126/science.aad5456, 2016.

Blacet, B. F. E., Heldman, J. D., and Heldman, J. D.: The photolysis of the aliphatic aldehydes. Acetaldehyde and iodine mixtures, J. Am. Chem. Soc., 64, 889–893, https://doi.org/10.1021/ja01256a044, 1942.

Blacet, F. E. and Calvert, J. G.: The photolysis of aliphatic aldehydes. XV. The butyraldehydes with iodine vapor, J. Am. Chem. Soc., 73, 667–674, https://doi.org/10.1021/ja01146a049, 1951.

675 Bowman, J. M. and Houston, P. L.: Theories and simulations of roaming, Chem. Soc. Rev., https://doi.org/10.1039/C7CS00578D, 2017.

Burak, I., Hepburn, J. W., Sivakumar, N., Hall, G. E., Chawla, G., and Houston, P. L.: State-to-state photodissociation dynamics of trans-glyoxal, J. Chem. Phys., 86, 1258–1268, https://doi.org/10.1063/1.452215, 1987.

Cady-Pereira, K. E., Chaliyakunnel, S., Shephard, M. W., Millet, D. B., Luo, M., and Wells, K. C.: HCOOH measurements from space: TES retrieval algorithm and observed global distribution, Atmos. Meas. Tech., 7, 2297–2311, https://doi.org/10.5194/amt-7-2297-2014, 2014.

680 Cao, J. and Xie, Z.-Z.: Internal conversion and intersystem crossing in α,β-enones: a combination of electronic structure calculations and dynamics simulations, Phys. Chem. Chem. Phys., 18, 6931–6945, https://doi.org/10.1039/c5cp06833a, 2016.

Carlier, P., Hannachi, H., and Mouvier, G.: The chemistry of carbonyl compounds in the atmosphere-A review, Atmos. Environ. (1967), 20, 2079–2099, https://doi.org/10.1016/0004-6981(86)90304-5, 1986.

Chen, S. L. and Fang, W. H.: Insights into photodissociation dynamics of acetaldehyde from ab initio calculations and molecular dynamics

685 simulations, J. Chem. Phys., 131, 054 306, https://doi.org/10.1021/jp073875+, 2009.

Chen, W. T., Shao, M., Lu, S. H., Wang, M., Zeng, L. M., Yuan, B., and Liu, Y.: Understanding primary and secondary sources of ambient carbonyl compounds in Beijing using the PMF model, Atmos. Chem. Phys., 14, 3047–3062, https://doi.org/10.5194/acp-14-3047-2014, 2014.

Chen, Y. and Zhu, L.: Wavelength-dependent photolysis of glyoxal in the 290-420 nm region, J. Phys. Chem. A, 107, 4643–4651,

690 https://doi.org/10.1021/jp022440d, 2003.

Clubb, A. E., Jordan, M. J. T., Kable, S. H., and Osborn, D. L.: Phototautomerization of acetaldehyde to vinyl alcohol: A primary process in UV-irradiated acetaldehyde from 295 to 335 nm, J. Phys. Chem. Lett., 3, 3522–3526, https://doi.org/10.1021/jz301701x, 2012.

Copeland, R. A. and Crosley, D. R.: Radiative, collisional and dissociative processes in triplet acetone, Chem. Phys. Lett., 115, 362–368, https://doi.org/10.1016/0009-2614(85)85149-6, 1985.

695 Couch, D. E., Nguyen, Q. L., Liu, A., Hickstein, D. D., Kapteyn, H. C., Murnane, M. M., and Labbe, N. J.: Detection of the keto-enol tautomerization in acetaldehyde, acetone, cyclohexanone, and methyl vinyl ketone with a novel VUV light source, Proc. Combust. Inst., 38, 1737–1744, https://doi.org/10.1016/j.proci.2020.06.139, 2021.

Cui, G. and Fang, W.: Mechanistic photodissociation of glycolaldehyde: Insights from ab initio and RRKM calculations, ChemPhysChem, 12, 1351–1357, https://doi.org/10.1002/cphc.201000968, 2011.

700 Diau, E. W.-G., Kötting, C., and Zewail, A. H.: Femtochemistry of Norrish Type-I reactions: I. Experimental and theoretical studies of acetone and related ketones on the S_1 surface, ChemPhysChem, 2, 273–293, https://doi.org/10.1002/1439-7641(20010518)2:5<273::AID-CPHC273>3.0.CO;2-H, 2001.

Dobeck, L. M., Lambert, H. M., Kong, W., Pisano, P. J., and Houston, P. L.: H_2 production in the 440-nm photodissociation of glyoxal, System, pp. 10 312–10 323, https://doi.org/10.1021/jp992333s, 1999.

705 Dykstra, C. E. and Schaefer, H. F.: Electronic structure of dicarbonyls. Glyoxal excited states, J. Am. Chem. Soc., 98, 401–406, https://doi.org/10.1021/ja00418a014, 1976.

Ehhalt, D. H. and Rohrer, F.: The tropospheric cycle of H_2: A critical review, Tellus B Chem. Phys. Meteorol., 61B, 500–535, https://doi.org/10.1111/j.1600-0889.2009.00416.x, 2009.

El-Sayed, M. A.: Spin-orbit coupling and the radiationless processes in nitrogen heterocyclics, Chem. Phys., 38, 2834–2838, 1961.

710 Franco, B., Blumenstock, T., Cho, C., Clarisse, L., Clerbaux, C., Coheur, P.-F., De Mazière, M., De Smedt, I., Dorn, H.-P., Emmerichs, T., Fuchs, H., Gkatzelis, G., Griffith, D. W. T., Gromov, S., Hannigan, J. W., Hase, F., Hohaus, T., Jones, N., Kerkweg, A., Kiendler-Scharr, A., Lutsch, E., Mahieu1, E., Novelli, A., Ortega, I., Paton-Walsh, C., Pommier, M., Pozzer, A., Reimer, D., Rosanka, S., Sander, R., Schneider, M., Strong, K., Tillmann, R., Van Roozendael, M., Vereecken, L., Vigouroux, C., Wahner, A., and Taraborrelli, D.: Ubiquitous atmospheric production of organic acids mediated by cloud droplets, Nature, 593, 233–237, https://doi.org/10.1038/s41586-021-03462-x,

715 2021.

Godunov, I. A., Yakovlev, N. N., and Khimii, Z. S.: Experimental structural and conformational studies of carbonyl molecules in the ground and lower excited states, J. Struct. Chem., 36, 238–253, https://doi.org/10.1007/BF02578062, 1995.

Goldstein, A. H. and Galbally, I. E.: Known and unexplored organic constituents in the earth's atmosphere, Environ. Sci. Technol., 41, 1514–1521, https://doi.org/10.1021/es072476p, 2007.

720 Goncharov, V., Herath, N., and Suits, A. G.: Roaming dynamics in acetone dissociation, J. Phys. Chem. A, 112, 9423–9428, https://doi.org/10.1021/jp802534r, 2008.

Grant, A., Witham, C. S., Simmonds, P. G., Manning, A. J., and O'Doherty, S.: A 15 year record of high-frequency, in situ measurements of hydrogen at Mace Head, Ireland, Atmos. Chem. Phys., 10, 1203–1214, https://doi.org/10.5194/acp-10-1203-2010, 2010.

Grimme, S., Antony, J., Ehrlich, S., Krieg, H., Grimme, S., Antony, J., Ehrlich, S., and Krieg, H.: A consistent and accurate ab ini-

725 tio parametrization of density functional dispersion correction (DFT-D) for the 94 elements H-Pu, J. Chem. Phys., 132, 154 104, https://doi.org/10.1063/1.3382344, 2010.

Grimme, S., Ehrlich, S., and Goerigk, L.: Effect of the damping function in dispersion corrected density functional theory, J. Comput. Chem., 32, 1456–1465, https://doi.org/10.1002/jcc.21759, 2011.

Gruver, J. T. and Calvert, J. G.: The vapor phase photolysis of (+)2-methylbutanal-iodine mixtures at wave length 3130 Å, J. Am. Chem.

730 Soc., 80, 3524–3527, https://doi.org/10.1021/ja01547a009, 1958.

Guo, S. J., Chen, M., He, X. L., Yang, W. W., and Tan, J. H.: Seasonal and diurnal characteristics of carbonyls in urban air in Qinzhou, China, Aerosol Air Qual. Res., 14, 1653–1664, https://doi.org/10.4209/aaqr.2013.12.0351, 2014.

Haas, Y.: Photochemical α-cleavage of ketones: Revisiting acetone, Photochem. Photobiol. Sci., 3, 6–16, https://doi.org/10.1039/b307997j, 2004.

735 Hansen, D. A. and Lee, E. K.: Radiative and nonradiative transitions in the first excited singlet state of simple linear aldehydes, J. Chem. Phys., 63, 3272–3277, https://doi.org/10.1063/1.431802, 1975.

Harrison, A. W., Kharazmi, A., Shaw, M. F., Quinn, M. S., Lee, K. L. K., Nauta, K., Rowell, K. N., Jordan, M. J. T., and Kable, S. H.: Dynamics and quantum yields of $H_2 + CH_2CO$ as a primary photolysis channel in CH_3CHO, Phys. Chem. Chem. Phys., pp. 14 284–14 295, https://doi.org/10.1039/c8cp06412a, 2019.

740 Hauglustaine, D. A.: A three-dimensional model of molecular hydrogen in the troposphere, J. Geophys. Res. Atmos., 107, 4330, https://doi.org/10.1029/2001JD001156, 2002.

Heazlewood, B. R., Jordan, M. J. T., Kable, S. H., Selby, T. M., Osborn, D. L., Shepler, B. C., Braams, B. J., and Bowman, J. M.: Roaming is the dominant mechanism for molecular products in acetaldehyde photodissociation, Proc. Natl. Acad. Sci. U.S.A., 105, 12 719–12 724, https://doi.org/10.1073/pnas.0802769105, 2008.

745 Heazlewood, B. R., Rowling, S. J., Maccarone, A. T., Jordan, M. J., and Kable, S. H.: Photochemical formation of HCO and CH_3 on the ground S_0 ($^1A'$) state of CH_3CHO, J. Chem. Phys., 130, 054 310, https://doi.org/10.1063/1.3070517, 2009.

27

Heazlewood, B. R., Maccarone, A. T., Andrews, D. U., Osborn, D. L., Harding, L. B., Klippenstein, S. J., Jordan, M. J. T., and Kable, S. H.: Near-threshold H/D exchange in CD$_3$CHO photodissociation, Nat. Chem., 3, 443–448, https://doi.org/10.1038/nchem.1052, 2011.

Heicklen, J. and Noyes, W. A.: The photolysis and fluorescence of acetone and acetone-biacetyl mixtures, J. Am. Chem. Soc., 81, 3858–3863, https://doi.org/10.1021/ja01524a016, 1959.

Hepburn, J. W., Buss, R. J., Butler, L. J., and Lee, Y. T.: Molecular beam study of the photochemistry of S_1 glyoxal, J. Phys. Chem., 87, 3638—3641, https://doi.org/10.1021/j100242a014, 1983.

Horowitz, A. and Calvert, J. G.: Wavelength dependence of the quantum efficiencies of the primary processes in formaldehyde photolysis at 25C, Int. J. Chem. Kinet., 10, 805–819, https://doi.org/10.1002/kin.550100803, 1978.

Horowitz, A. and Calvert, J. G.: Wavelength dependence of the primary processes in acetaldehyde photolysis, J. Phys. Chem., 86, 3105–3114, https://doi.org/10.1021/j100213a011, 1982.

Houston, P. L. and Kable, S. H.: Photodissociation of acetaldehyde as a second example of the roaming mechanism, Proc. Natl. Acad. Sci. U.S.A., 103, 16 079–16 082, https://doi.org/10.1073/pnas.0604441103, 2006.

Jenkin, M. E., Saunders, S. M., and Pilling, M. J.: The tropospheric degradation of volatile organic compounds: A protocol for mechanism development, Atmos. Environ., 31, 81–104, https://doi.org/10.1016/S1352-2310(96)00105-7, 1997.

Jenkin, M. E., Saunders, S. M., Derwent, R. G., and Pilling, M. J.: Development of a reduced speciated VOC degradation mechanism for use in ozone models, https://doi.org/10.1016/S1352-2310(02)00563-0, 2002.

Kahan, T. F., Ormond, T. K., Ellison, G. B., and Vaida, V.: Acetic acid formation via the hydration of gas-phase ketene under ambient conditions, Chem. Phys. Lett., 565, 1–4, https://doi.org/10.1016/j.cplett.2013.02.030, 2013.

Kao, C. C., Ho, M.-L., Chen, M.-W., Lee, S.-J., and Chen, I.-C.: Internal state distributions of fragment HCO via S_0 and T_1 pathways of glyoxal after photolysis in the ultraviolet region, J. Chem. Phys, 120, 5087–5095, https://doi.org/10.1063/1.1647538, 2004.

Karton, A., Tarnopolsky, A., Lamère, J.-F., Schatz, G. C., and Martin, J. M. L.: Highly accurate first-principles benchmark data sets for the parametrization and validation of density functional and other approximate methods. Derivation of a robust, generally applicable, double-hybrid functional for thermochemistry and thermochemical kinetics, J. Phys. Chem. A, 112, 12 868, https://doi.org/10.1021/jp801805p, 2008.

Kawamura, K., Steinberg, S., and Kaplan, I. R.: Homologous series of C1-C10 monocarboxylic acids and C1-C6 carbonyls in Los Angeles air and motor vehicle exhausts, Atmos. Environ., 34, 4175–4191, https://doi.org/10.1016/S1352-2310(00)00212-0, 2000.

Keeffe, J. R., Kresge, A. J., and Schepp, N. P.: Generation of simple enols by photooxidation. Keto-enol equilibrium constants of some aliphatic systems in aqueous solution, J. Am. Chem. Soc., 110, 1993–1995, https://doi.org/10.1021/ja00214a069, 1988.

Kesharwani, M. K., Brauer, B., and Martin, J. M.: Frequency and zero-point vibrational energy scale factors for double-hybrid density functionals (and other selected methods): Can anharmonic force fields be avoided?, J. Phys. Chem. A, 119, 1701–1714, https://doi.org/10.1021/jp508422u, 2015.

Kesselmeier, J. and Staudt, M.: Biogenic volatile organic compunds (VOC): An overview on emission, physiology and ecology., J. Atmos. Chem., 33, 23–88, https://doi.org/10.1023/A:1006127516791, 1999.

Kharazmi, A.: Investigating the complex photochemistry of atmospheric carbonyls, Ph.D. thesis, The University of New South Wales, 2019.

Kirkbride, F. W. and Norrish, R. G. W.: The photochemical properties of the carbonyl group, Trans. Faraday Soc., 27, 404–408, https://doi.org/10.1039/TF9312700404, 1931.

Lary, D. J. and Shallcross, D. E.: Central role of carbonyl compounds in atmospheric chemistry, J. Geophys. Res. Atmos., 105, 19 771–19 778, https://doi.org/10.1029/1999JD901184, 2000.

785   Lee, A. M. D., Coe, J. D., Ullrich, S., Ho, M. L., Lee, S. J., Cheng, B. M., Zgierski, M. Z., Chen, I. C., Martinez, T. J., and Stolow, A.: Substituent effects on dynamics at conical intersections: α,β-enones, J. Phys. Chem. A, 111, 11 948–11 960, https://doi.org/10.1021/jp074622j, 2007.

Lee, K. L. K., Quinn, M. S., Maccarone, A. T., Nauta, K., Houston, P. L., Reid, S. A., Jordan, M. J., and Kable, S. H.: Two roaming pathways in the photolysis of CH_3CHO between 328 and 308 nm, Chem. Sci., 5, 4633–4638, https://doi.org/10.1039/c4sc02266a, 2014.

790   Lee, K. L. K., Nauta, K., and Kable, S. H.: Photodissociation of acetone from 266 to 312 nm: Dynamics of $CH_3 + CH_3CO$ channels on the S_0 and T_1 states, J. Chem. Phys., 146, 044 304, https://doi.org/10.1063/1.4974035, 2017.

Lee, S. H. and Chen, I. C.: Non-exponential decays of the S_1 vibronic levels of acetaldehyde, Chem. Phys., 220, 175–189, https://doi.org/10.1016/S0301-0104(97)00148-1, 1997.

Lee, Y., Zhou, X., Kleinman, L. I., Nunnermacker, L. J., Springston, S. R., Daum, P. H., Newman, L., Keigley, W. G., Holdren, M. W.,
795   Spicer, C. W., Young, V., Fu, B., Parrish, D. D., Holloway, J., Williams, J., Roberts, J. M., Ryerson, T. B., and Fehsenfeld, F. C.: Atmospheric chemistry and distribution of formaldehyde and several multioxygenated carbonyl compounds during the 1995 Nashville/Middle Tennessee Ozone Study, J. Geophys. Res. Atmos., 103, https://doi.org/10.1029/98JD01251, 1998.

Liu, J.-Y., Long, Z.-W., Mitchell, E., and Long, B.: New mechanistic pathways for the reactions of formaldehyde with formic acid catalyzed by sulfuric acid and formaldehyde with sulfuric acid catalyzed by formic acid: Formation of potential secondary organic aerosol precursors,
800   ACS Earth Space Chem. Article ASAP, https://doi.org/10.1021/acsearthspacechem.1c00002, 2021.

Loge, G. W. and Parmenter, C. S.: Collision-free dissociation after excitation of single rotational levels in S_1 glyoxal, J. Phys. Chem., 85, 1653–1662, https://doi.org/10.1021/j150612a011, 1981.

Mauguière, F. A. L., Collins, P., Kramer, Z. C., Carpenter, B. K., Ezra, G. S., Farantos, S. C., and Wiggins, S.: Phase space structures explain hydrogen atom roaming in formaldehyde decomposition, J. Phys. Chem. Lett., 6, 4123–4128, https://doi.org/10.1021/acs.jpclett.5b01930,
805   2015.

Menchaca-Torre, H. L., Mercado-Hernández, R., Rodríguez-Rodríguez, J., and Mendoza-Domínguez, A.: Diurnal and seasonal variations of carbonyls and their effect on ozone concentrations in the atmosphere of Monterrey, Mexico, J. Air Waste Manag. Assoc., 65, 500–510, https://doi.org/10.1080/10962247.2015.1005849, 2015.

Millet, D. B., Guenther, A., Siegel, D., Nelson, N., Singh, H., De Gouw, J., Warneke, C., Williams, J., Eerdekens, G., Sinha, V., Karl, T.,
810   Flocke, F., Apel, E., Riemer, D. D., Palmer, P. I., and Barkley, M.: Global atmospheric budget of acetaldehyde: 3-D model analysis and constraints from in-situ and satellite observations, Atmos. Chem. Phys., 10, 3405–3425, https://doi.org/10.5194/acp-10-3405-2010, 2010.

Millet, D. B., Baasandorj, M., Farmer, D. K., Thornton, J. A., Baumann, K., Brophy, P., Chaliyakunnel, S., de Gouw, J. A., Graus, M., Hu, L., Koss, A., Lee, B. H., Lopez-Hilfiker, F. D., Neuman, J. A., Paulot, F., Peischl, J., Pollack, I. B., Ryerson, T. B., Warneke, C., Williams, B. J., and Xu, J.: A large and ubiquitous source of atmospheric formic acid, Atmos. Chem. Phys., 15, 6283–6304, https://doi.org/10.5194/acp-
815   15-6283-2015, 2015.

Moortgat, G. K. and Warneck, P.: CO and H_2 quantum yields in the photodecomposition of formaldehyde in air, J. Chem. Phys., 70, 3639–3651, https://doi.org/10.1063/1.437956, 1979.

Moortgat, G. K., Seiler, W., and Warneck, P.: Photodissociation of HCHO in air: CO and H_2 quantum yields at 220 and 300 K, J. Chem. Phys., 78, 1185–1190, https://doi.org/10.1063/1.444911, 1983.

820   Moortgat, G. K., Meyrahn, H., and Warneck, P.: Photolysis of acetaldehyde in air: CH_4, CO and CO_2 quantum yields, ChemPhysChem, 11, 3896–3908, https://doi.org/10.1002/cphc.201000757, 2010.

29

Morajkar, P., Bossolasco, A., Schoemaecker, C., and Fittschen, C.: Photolysis of CH_3CHO at 248 nm: Evidence of triple fragmentation from primary quantum yield of CH_3 and HCO radicals and H atoms, J. Chem. Phys., 140, 214 308, https://doi.org/10.1063/1.4878668, 2014.

Neese, F.: Software update: The ORCA program system, version 4.0, Wiley Interdiscip. Rev. Comput. Mol. Sci, 8, 4–9, https://doi.org/10.1002/wcms.1327, 2017.

Norrish, R. G. W. and Appleyard, M. E. S.: 191. Primary photochemical reactions. Part IV. Decomposition of methyl ethyl ketone and methyl butyl ketone, J. Chem. Soc., pp. 874–880, https://doi.org/10.1039/JR9340000874, 1934.

Novelli, P. C.: Molecular hydrogen in the troposphere: Global distribution and budget, J. Geophys. Res. Atmos., 104, 30 427–30 444, https://doi.org/10.1029/1999JD900788, 1999.

Pal, R., Kim, K. H., Hong, Y. J., and Jeon, E. C.: The pollution status of atmospheric carbonyls in a highly industrialized area, J. Hazard. Mater., 153, 1122–1135, https://doi.org/10.1016/j.jhazmat.2007.09.068, 2008.

Patterson, J. D., Aydin, M., Crotwell, A. M., Petron, G., Severinghaus, J. P., and Saltzman, E. S.: Atmospheric history of H_2 over the past century reconstructed from South Pole firn air, Geophys. Res. Lett., 47, e2020GL087 787, https://doi.org/10.1029/2020GL087787, 2020.

Pople, J. A.: Quantum chemical models (Nobel lecture), Angew. Chem. Int. Ed., 38, 1894–1902, https://doi.org/10.1002/(SICI)1521-3773(19990712)38:13/14<1894::AID-ANIE1894>3.0.CO;2-H, 1999.

Price, H., Jaeglé, L., Rice, A., Quay, P., Novelli, P. C., and Gammon, R.: Global budget of molecular hydrogen and its deuterium content: Constraints from ground station, cruise, and aircraft observations, J. Geophys. Res. Atmos., 112, D22 108, https://doi.org/10.1029/2006JD008152, 2007.

Quinn, M. S., Andrews, D. U., Nauta, K., Jordan, M. J., and Kable, S. H.: The energy dependence of CO(v,J) produced from H 2 CO via the transition state, roaming, and triple fragmentation channels, J. Chem. Phys., 147, https://doi.org/10.1063/1.4983138, 2017.

Raber, W. H. and Moortgat, G. K.: Photooxidation of selected carbonyl compounds in air: methyl ethyl ketone, methyl vinyl ketone, methacrolein and methylglyoxal, in: Progress and Problems in Atmospheric Chemistry, edited by Barker, R. J., pp. 318–373, World Scientific Publishing Company, Singapore, 1996.

Rhee, T. S., Brenninkmeijer, C. A., and Röckmann, T.: The overwhelming role of soils in the global atmospheric hydrogen cycle, Atmos. Chem. Phys., 6, 1611–1625, https://doi.org/10.5194/acp-6-1611-2006, 2006.

Rickard, A. and Young, J.: The Master Chemical Mechanism (MCM) v3.2, http://mcm.leeds.ac.uk/MCM.

Rowell, K. N., Kable, S. H., and Jordan, M. J. T.: Structural effects on the Norrish Type I α-bond cleavage of tropospherically important carbonyls, J. Phys. Chem. A, 123, 10 381–10 396, https://doi.org/10.1021/acs.jpca.9b05534, 2019.

Rubio-Lago, L., Amaral, G. A., Arregui, A., González-Vázquez, J., and Bañares, L.: Imaging the molecular channel in acetaldehyde photodissociation: Roaming and transition state mechanisms, Phys. Chem. Chem. Phys., 14, 6067–6078, https://doi.org/10.1039/c2cp22231k, 2012.

Ruscic, B., Pinzon, R. E., Von Laszewski, G., Kodeboyina, D., Burcat, A., Leahy, D., Montoy, D., and Wagner, A. F.: Active thermochemical tables: Thermochemistry for the 21st century, J. Phys. Conf. Ser., 16, 561–570, https://doi.org/10.1088/1742-6596/16/1/078, 2005.

Ruscic, B. and Bross, D. H.: Active thermochemical tables (ATcT) values based on ver. 1.122p of the Thermochemical Network, https://atct.anl.gov/, 2020.

Saheb, V. and Zokaie, M.: Multichannel gas-phase unimolecular decomposition of acetone: Theoretical kinetic studies, J. Phys. Chem. A, 122, 5895–5904, https://doi.org/10.1021/acs.jpca.8b02423, 2018.

Salter, R. J., Blitz, M. a., Heard, D. E., Pilling, M. J., and Seakins, P. W.: Pressure and temperature dependent photolysis of glyoxal in the 355-414 nm region: evidence for dissociation from multiple states., Phys. Chem. Chem. Phys., 15, 6516–26, https://doi.org/10.1039/c3cp43596b, 2013.

Schalk, O., Schuurman, M. S., Wu, G., Lang, P., Mucke, M., Feifel, R., and Stolow, A.: Internal conversion versus intersystem crossing: What drives the gas phase dynamics of cyclic α,β-enones?, J. Phys. Chem. A, 118, 2279–2287, https://doi.org/10.1021/jp4124937, 2014.

Schuurman, M. S. and Stolow, A.: Dynamics at conical intersections, Annu. Rev. Phys. Chem., 69, 427–450, https://doi.org/10.1146/annurev-physchem-052516-050721, 2018.

Seco, R., Peñuelas, J., and Filella, I.: Short-chain oxygenated VOCs: Emission and uptake by plants and atmospheric sources, sinks, and concentrations, Atmos. Environ., 41, 2477–2499, https://doi.org/10.1016/j.atmosenv.2006.11.029, 2007.

Shaw, M. F., Sztáray, B., Whalley, L. K., Heard, D. E., Millet, D. B., Jordan, M. J., Osborn, D. L., and Kable, S. H.: Photo-tautomerization of acetaldehyde as a photochemical source of formic acid in the troposphere, Nat. Commun., 9, 1–7, https://doi.org/10.1038/s41467-018-04824-2, 2018.

Simon, H., Beck, L., Bhave, P. V., Divita, F., Hsu, Y., Luecken, D., Mobley, J. D., Pouliot, G. A., Reff, A., Sarwar, G., and et al.: The development and uses of EPA's SPECIATE database, Atmos. Pollut. Res., 1, 196–206, https://doi.org/10.5094/apr.2010.026, 2010.

Skorobogatov, G. A., Meilakhs, A. G., Pogosyan, Y. I., and Khripun, V. K.: New mechanism of photodissociation of gaseous acetone, Russ. J. Gen. Chem., 72, 1271–1275, https://doi.org/10.1023/a:1020896200573, 2002.

So, S., Wille, U., and da Silva, G.: Atmospheric chemistry of enols: A theoretical study of the vinyl alcohol + OH + O_2 reaction mechanism, Environ. Sci. Technol., 48, 6694–6701, https://doi.org/10.1021/es500319q, 2014.

So, S., Wille, U., and Da Silva, G.: A theoretical study of the photoisomerization of glycolaldehyde and subsequent OH radical-initiated oxidation of 1,2-ethenediol, J. Phys. Chem. A, 119, 9812–9820, https://doi.org/10.1021/acs.jpca.5b06854, 2015.

So, S., Wille, U., and Da Silva, G.: Photoisomerization of methyl vinyl ketone and methacrolein in the troposphere: A theoretical investigation of ground-State reaction pathways, ACS Earth Space Chem., 2, 753–763, https://doi.org/10.1021/acsearthspacechem.8b00066, 2018.

Tadić, J. M., Juranić, I. O., and Moortgat, G. K.: Photooxidation of n-heptanal in air: Norrish type I and II processes and quantum yield total pressure dependency, J. Chem. Soc. Perkin Trans. 2, 2, 135–140, https://doi.org/10.1039/b106476m, 2002.

Tadić, J. M., Moortgat, G. K., Bera, P. P., Loewenstein, M., Yates, E. L., and Lee, T. J.: Photochemistry and photophysics of n-butanal, 3-methylbutanal, and 3,3-dimethylbutanal: Experimental and theoretical study, J. Phys. Chem. A, 116, 5830–5839, https://doi.org/10.1021/jp208665v, 2012.

Tanner, R. L., Zielinska, B., Uberna, E., Harshfield, G., and McNichol, A. P.: Concentrations of carbonyl compounds and the carbon isotopy of formaldehyde at a coastal site in Nova Scotia during the NARE summer intensive, J. Geophys. Res. Atmos., 101, 28 961–28 970, https://doi.org/10.1029/95jd03574, 1996.

Toulson, B. W., Kapnas, K. M., Fishman, D. A., and Murray, C.: Competing pathways in the near-UV photochemistry of acetaldehyde, Phys. Chem. Chem. Phys., 19, 14 276–14 288, https://doi.org/10.1039/c7cp02573d, 2017.

Toulson, B. W., Fishman, D. A., and Murray, C.: Photodissociation dynamics of acetone studied by time-resolved ion imaging and photofragment excitation spectroscopy, Phys. Chem. Chem. Phys., 20, 2457–2469, https://doi.org/10.1039/C7CP07320H, 2018.

Townsend, D., Lahankar, S. A., Lee, S. K., Chambreau, S. D., Suits, A. G., Zhang, X., Rheinecker, J., Harding, L. B., and Bowman, J. M.: The roaming atom: Straying from the reaction path in formaldehyde decomposition, Science, 306, 1158–1161, https://doi.org/10.1126/science.1104386, 2004.

895   Tröstl, J., Chuang, W. K., Gordon, H., Heinritzi, M., Yan, C., Molteni, U., Ahlm, L., Frege, C., Bianchi, F., Wagner, R., Simon, M., Lehtipalo, K., Williamson, C., Craven, J. S., Duplissy, J., Adamov, A., Almeida, J., Bernhammer, A. K., Breitenlechner, M., Brilke, S., Dias, A., Ehrhart, S., Flagan, R. C., Franchin, A., Fuchs, C., Guida, R., Gysel, M., Hansel, A., Hoyle, C. R., Jokinen, T., Junninen, H., Kangasluoma, J., Keskinen, H., Kim, J., Krapf, M., Kürten, A., Laaksonen, A., Lawler, M., Leiminger, M., Mathot, S., Möhler, O., Nieminen, T., Onnela, A., Petäjä, T., Piel, F. M., Miettinen, P., Rissanen, M. P., Rondo, L., Sarnela, N., Schobesberger, S., Sengupta, K., Sipilä, M., Smith,

900   J., Steiner, G., Tomè, A., Virtanen, A., Wagner, A. C., Weingartner, E., Wimmer, D., Winkler, P. M., Ye, P., Carslaw, K. S., Curtius, J., Dommen, J., Kirkby, J., Kulmala, M., Riipinen, I., Worsnop, D. R., Donahue, N. M., and Baltensperger, U.: The role of low-volatility organic compounds in initial particle growth in the atmosphere, Nature, 533, 527–31, https://doi.org/10.1038/nature18271, 2016.

Tsai, P.-Y., Li, H.-K., Kasai, T., and Lin, K.-C.: Roaming as the dominant mechanism for molecular products in the photodissociation of large aliphatic aldehydes, Phys. Chem. Chem. Phys., 17, 23112–23120, https://doi.org/10.1039/C5CP03408F, 2015.

905   Valachovic, L. R., Tuchler, M. F., Dulligan, M., Droz-Georget, T., Zyrianov, M., Kolessov, A., Reisler, H., and Wittig, C.: Photoiniti-ated H_2CO unimolecular decomposition: Accessing H + HCO products via S_0 and T_1 pathways, J. Chem. Phys., 112, 2752–2761, https://doi.org/10.1063/1.480849, 2000.

Vigouroux, C., Hendrick, F., Stavrakou, T., Dils, B., De Smedt, I., Hermans, C., Merlaud, A., Scolas, F., Senten, C., Vanhaelewyn, G., Fally, S., Carleer, M., Metzger, J.-M., Müller, J.-F., Van Roozendael, M., and De Mazière, M.: Ground-based FTIR and MAX-DOAS

910   observations of formaldehyde at Réunion Island and comparisons with satellite and model data, Atmos. Chem. Phys., 9, 9523–9544, https://doi.org/10.5194/acp-9-9523-2009, 2009.

Wagner, P. J. and Klán, P.: Norrish type II photoelimination of ketones: Cleavage of 1,4-biradicals formed by γ-hydrogen abstraction, in: CRC Handbook of Organic Photochemistry and Photobiology, 2nd Edition, edited by Horspool, W. M. and Lenci, F., chap. 52, pp. 1–22, CRC Press, Boca Raton, 2004.

915   Wagner, P. J. and Zepp, R. G.: Trapping by mercaptans of biradical intermediates in type II photoelemination, J. Am. Chem. Soc., 94, 287, https://doi.org/10.1021/ja00756a057, 1972.

Wallington, T. J., Ammann, M., Cox, R. A., Crowley, J. N., Herrmann, H., Jenkin, M. E., McNeill, V., Mellouki, A., and Troe, J.: IUPAC task group on atmospheric chemical kinetic data evaluation, http://iupac.pole-ether.fr/, 2018.

Warneck, P. and Moortgat, G. K.: Quantum yields and photodissociation coefficients of acetaldehyde in the troposphere, Atmos. Environ.,

920   62, 153–163, https://doi.org/10.1016/j.atmosenv.2012.08.024, 2012.

Weigend, F. and Ahlrichs, R.: Balanced basis sets of split valence, triple zeta valence and quadruple zeta valence quality for H to Rn: Design and assessment of accuracy., Phys. Chem. Chem. Phys., 7, 3297–305, https://doi.org/10.1039/b508541a, 2005.

Whangbo, M. H. and Stewart, K. R.: On the thermodynamic stability and reactivity of alkyl-substituted alkenes, J. Org. Chem., 47, 736–738, https://doi.org/10.1021/jo00343a028, 1982.

925   Wild, O., Zhu, X., and Prather, M. J.: Fast-J: Accurate simulation of in- and below-cloud photolysis in tropospheric chemical models, J. Atmos. Chem., 37, 245–282, https://doi.org/10.1023/A:1006415919030, 2000.

Xiao, X., Prinn, R. G., Simmonds, P. G., Steele, L. P., Novelli, P. C., Huang, J., Langenfelds, R. L., O'Doherty, S., Krummel, P. B., Fraser, P. J., Porter, L. W., Weiss, R. F., Salameh, P., and Wang, R. H. J.: Optimal estimation of the soil uptake rate of molec-ular hydrogen from the advanced global atmospheric gases experiment and other measurements, J. Geophys. Res., 112, D07303,

930   https://doi.org/10.1029/2006JD007241, 2007.

Yang, C., Bhattacharyya, S., Liu, L., Fang, W.-H., and Liu, K.: Real-time tracking of the entangled pathways in the multichannel photodis-sociation of acetaldehyde, Phys. Chem. Chem. Phys., 11, 6423–6430, 2020.

Yang, X., Xue, L., Wang, T., Wang, X., Gao, J., Lee, S., Blake, D. R., Chai, F., and Wang, W.: Observations and explicit modeling of summertime carbonyl formation in Beijing: Identification of key precursor species and their impact on atmospheric oxidation chemistry, J. Geophys. Res. Atmos., 123, 1426–1440, https://doi.org/10.1002/2017jd027403, 2018.

Yashiro, H., Sudo, K., Yonemura, S., and Takigawa, M.: The impact of soil uptake on the global distribution of molecular hydrogen: chemical transport model simulation, Atmos. Chem. Phys., 11, 6701–6719, https://doi.org/10.5194/acp-11-6701-2011, 2011.

Yuan, B., Veres, P. R., Warneke, C., Roberts, J. M., Gilman, J. B., Koss, A., Edwards, P. M., Graus, M., Kuster, W. C., Li, S.-M., Wild, R. J., Brown, S. S., Dubé, W. P., Lerner, B. M., Williams, E. J., Johnson, J. E., Quinn, P. K., Bates, T. S., Lefer, B., Hayes, P. L., Jimenez, J. L., Weber, R. J., Zamora, R., Ervens, B., Millet, D. B., Rappenglück, B., and de Gouw, J. A.: Investigation of secondary formation of formic acid: Urban environment vs. oil and gas producing region, Atmos. Chem.and Phys., 15, 1975–1993, https://doi.org/10.5194/acp-15-1975-2015, 2015.

Zahra, A. and Noyes, W. A.: The photochemistry of methyl isopropyl ketone, J. Phys. Chem., 69, 943–948, https://doi.org/10.1021/j100887a041, 1965.

Zhang, R., Suh, I., Zhao, J., Zhang, D., Fortner, E. C., Tie, X., Molina, L. T., and Molina, M. J.: Atmospheric new particle formation enhanced by organic acids, Science, 304, 1487–1490, https://doi.org/10.1126/science.1095139, 2004.

Zhu, C. and Zhu, L.: Photolysis of glycolaldehyde in the 280–340 nm region, J. Phys. Chem. A, 114, 8384–8390, https://doi.org/10.1021/jp104497d, 2010.

Zhu, L., Tang, Y., Chen, Y., and Cronin, T.: Wavelength-dependent photolysis of C3-C7 aldehydes in the 280-330 nm region, Spectrosc. Lett., 42, 467–478, https://doi.org/10.1080/00387010903267195, 2009.
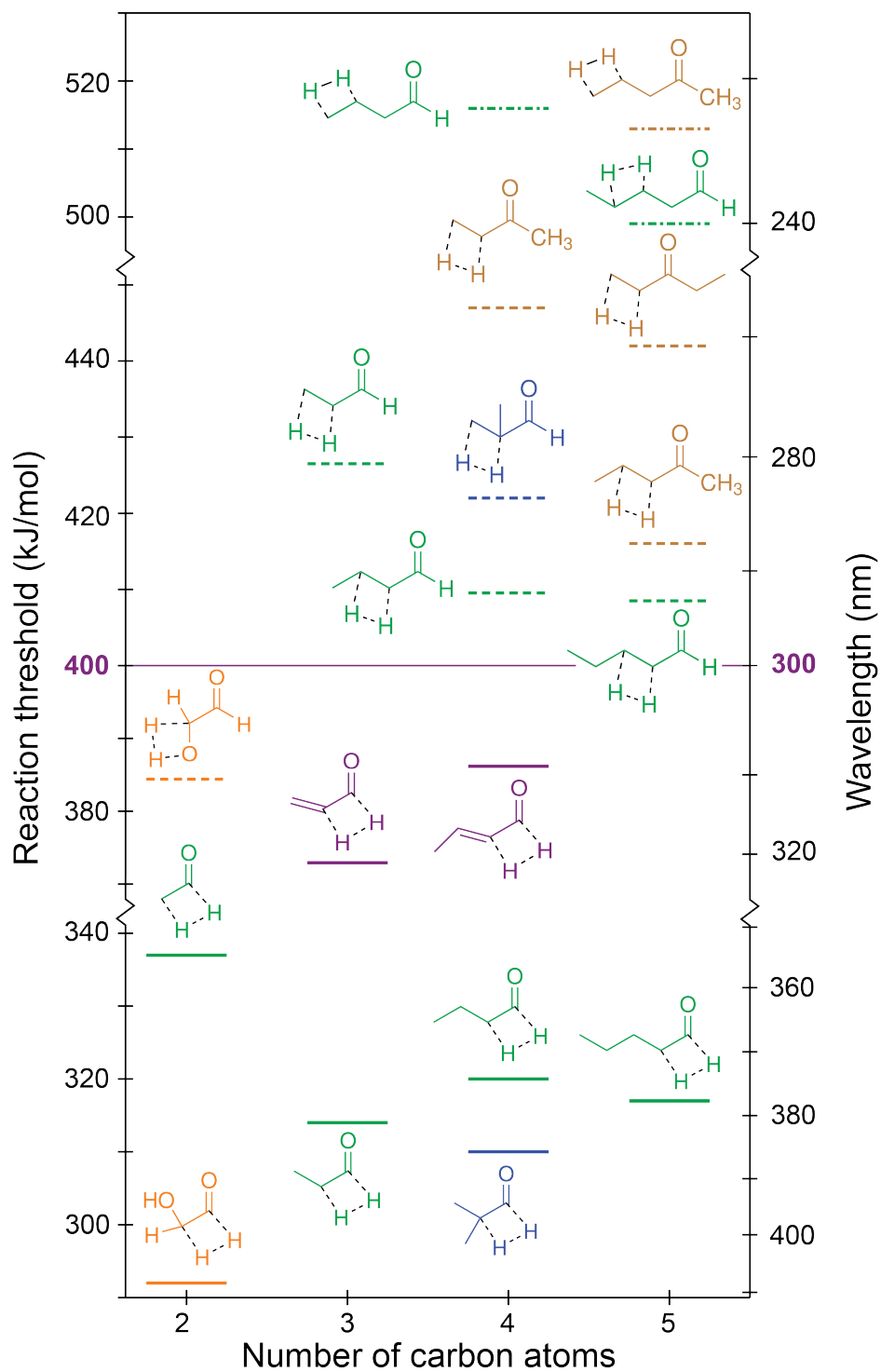
Figure 7. Zero-point vibrational energy corrected B2GP-PLYP-D3/def2-TZVP S_0 H_2–loss thresholds. *Solid lines*: formyl–H + α–H; *Dashed lines*: α–H + β–H; *Dot-dashed lines*: β–H + γ–H.
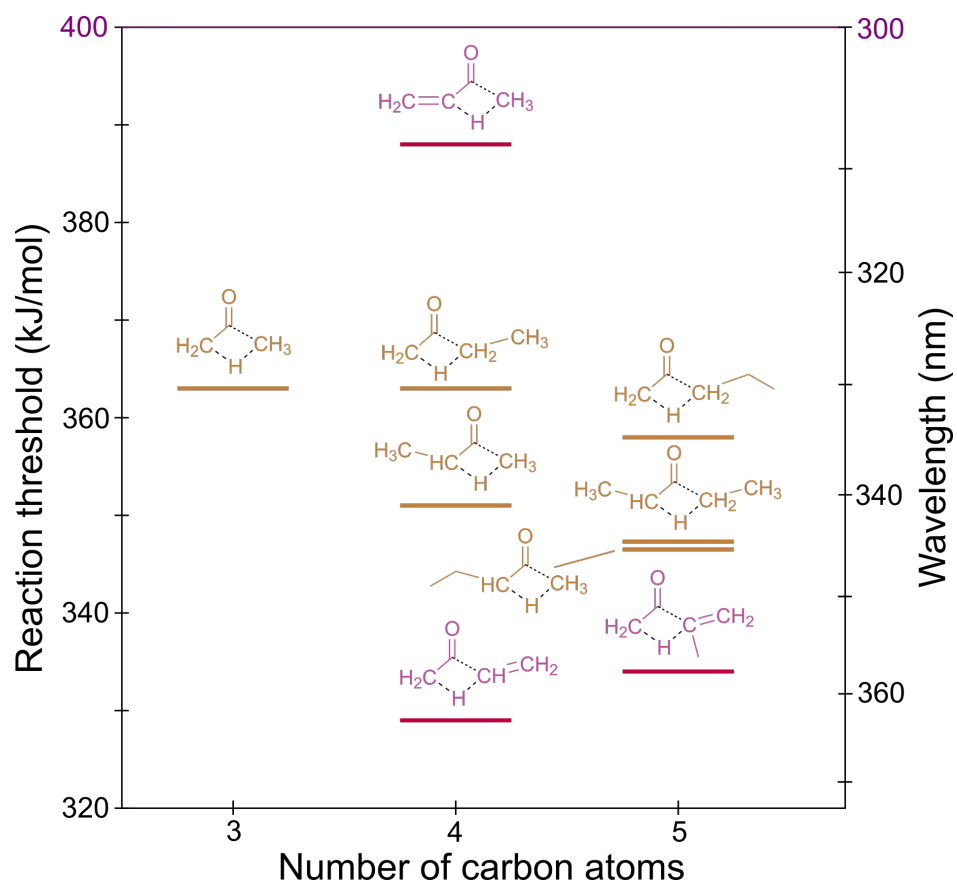
Figure 8. Zero-point vibrational energy corrected B2GP-PLYP-D3/def2-TZVP S_0 alkane/alkene elimination thresholds.
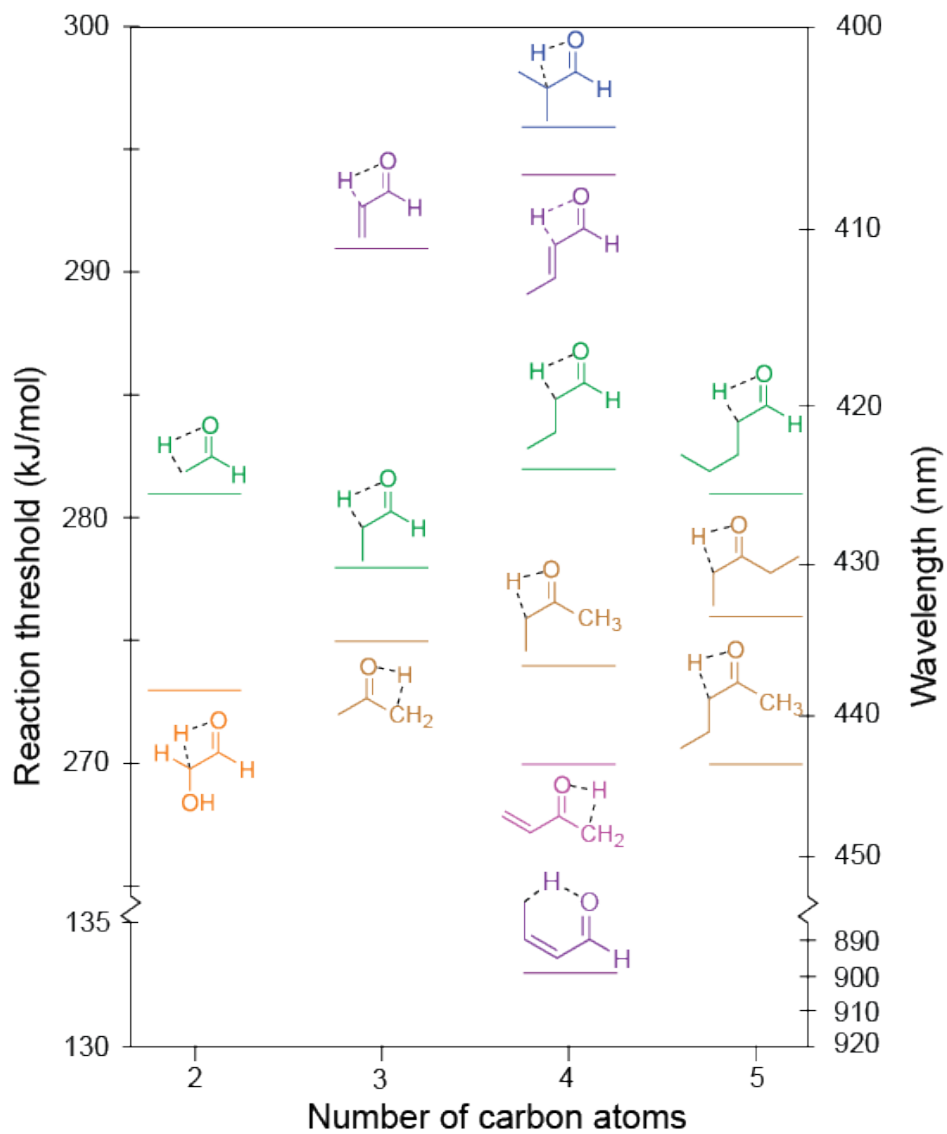
Figure 9. Zero-point vibrational energy corrected B2GP-PLYP-D3/def2-TZVP S_0 keto–enol tautomerisation thresholds.
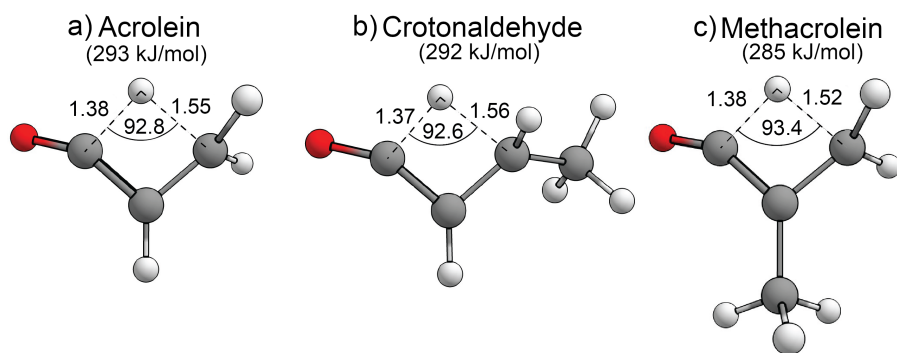
Figure 10. Optimised B2GP-PLYP-D3/def2-TZVP S_0 TSs and zero-point vibrational energy corrected threshold energies for enal–ketene tautomerisation, as shown. Key structural parameters in Å and degrees.